AGU PUBLICATIONS

Tectonics

RESEARCH ARTICLE
10.1002/2013TC003319

Key Points:
- Crustal structure beneath the Tajo Basin in central Spain
- Strong north-south lower crust differences
- Tectonic emplacement of low velocity-low resistivity in midcrust

Correspondence to:
A. G. Jones,
alan@cp.dias.ie

Citation:
Schmoldt, J.-P., A. G. Jones, and O. Rosell (2014), Structures and geometries of the Tajo Basin crust, Spain: Results of a magnetotelluric investigation compared to seismic and thermal models, *Tectonics*, *33*, 1710–1737, doi:10.1002/2013TC003319.

Received 21 FEB 2013
Accepted 11 AUG 2014
Accepted article online 18 AUG 2014
Published online 18 SEP 2014

Structures and geometries of the Tajo Basin crust, Spain: Results of a magnetotelluric investigation compared to seismic and thermal models

J.-P. Schmoldt[1,2], A. G. Jones[1], and O. Rosell[3]

[1]Geophysics Section, School of Cosmic Physics, Dublin Institute for Advanced Studies, Dublin, Ireland, [2]Department of Earth and Ocean Sciences, School of Natural Sciences, National University of Ireland, Galway, Galway, Ireland, [3]Departament de Geodinàmica i Geofísica, Facultat de Geologia, Universitat de Barcelona, Barcelona, Spain

Abstract The Tajo Basin and Betic Mountain Chain in the south central region of the Iberian Peninsula were chosen for investigation in the first phase of the magnetotelluric (MT) component of the PICASSO (Program to Investigate the Convective Alboran Sea System Overturn) project. The MT results provide information about the electrical conductivity distribution in previously unprobed subsurface regions, as well as complimenting and enhancing results of prior geological and geophysical investigations thereby enabling the definition of a petrological subsurface model and a comprehensive understanding about the tectonic setting. Two-dimensional (2-D) inversion of the MT data provides enhanced insight into Iberian subsurface geology in the crust. The most striking features of the final model are (i) a distinct vertical interface within the Variscan basement beneath the center of the Tajo Basin that is spatially associated with the boundary between regions with and without substantial Alpine deformation, and (ii) a middle to lower crustal conductive anomaly that can be related to remnants of asthenospheric intrusion in connection with Pliocene volcanic events in the Calatrava Volcanic Province. For the latter, effects of hydrous phases are inferred that may originate from dehydration processes within the subducting slab beneath Alboran Domain and Betic Mountain Chain.

1. Introduction

The Iberian Peninsula is the westernmost extent of the Eurasian continent, bounded by the Pyrenees to the northeast, the Bay of Biscay to the northwest, the Atlantic Ocean to the west and southwest, and the Mediterranean Sea to the south and southeast (Figure 1). Surprisingly, especially given its enigmatic high elevation [e.g., *Casas-Sainz and de Vicente*, 2009], the central region of the Iberian Peninsula has remained comparatively neglected in terms of lithospheric-scale investigations. Previous studies, particularly of deep-seated structures, have mostly focused on the borders of the peninsula, namely the Pyrenees [e.g., *Ledo et al.*, 2000], Cantabrian Mountains [e.g., *Gallart et al.*, 1995; *Pulgar et al.*, 1996], and the Betic Mountain Chain [e.g., *Serrano et al.*, 1998; *Pous et al.*, 1999; *Martí*, 2007; *Martí et al.*, 2009; *Rosell et al.*, 2011; *Ruiz-Constán et al.*, 2010] as well as on parts of the Iberian Massif in the southwest of Iberia [e.g., *Carbonell et al.*, 1998; *Pous et al.*, 2004; *Muñoz et al.*, 2005, 2008]. A receiver function study of the Ebro Basin subsurface in NE Spain was carried out by *Julià et al.* [1998], and deeper structures of central Iberian regions have been determined mainly by large-scale seismic tomography studies [e.g., *Bijwaard and Spakman*, 2000; *Amaru et al.*, 2008; *Koulakov et al.*, 2009], with models exhibiting low resolution for the Spanish subsurface. Other studies are currently still at the stage of ongoing work, e.g., *Pous et al.* [2011], which stretch from San Vicente de la Barquera in the Cantabrian Sea to Malaga and *Seillé et al.* [2012], located in the Iberian Chain and are not yet published in peer-reviewed journals.

This paper reports on work undertaken to probe central Spain utilizing the magnetotelluric (MT) method, which uses time variations of the electromagnetic field in order to determine the lateral and vertical distribution of electrical conductivity at crust and mantle depths. Information from MT enhances knowledge of geological setting, not only by providing detailed geometrical information about local subsurface regions that previously were not well resolved but also by yielding an additional parameter that augments other physical (e.g., seismic or thermal) parameters in order to be able to draw firmer conclusions about mantle petrology [e.g., *Jones et al.*, 2009; *Fullea et al.*, 2011]. Electrical conductivity is highly sensitive to changes in

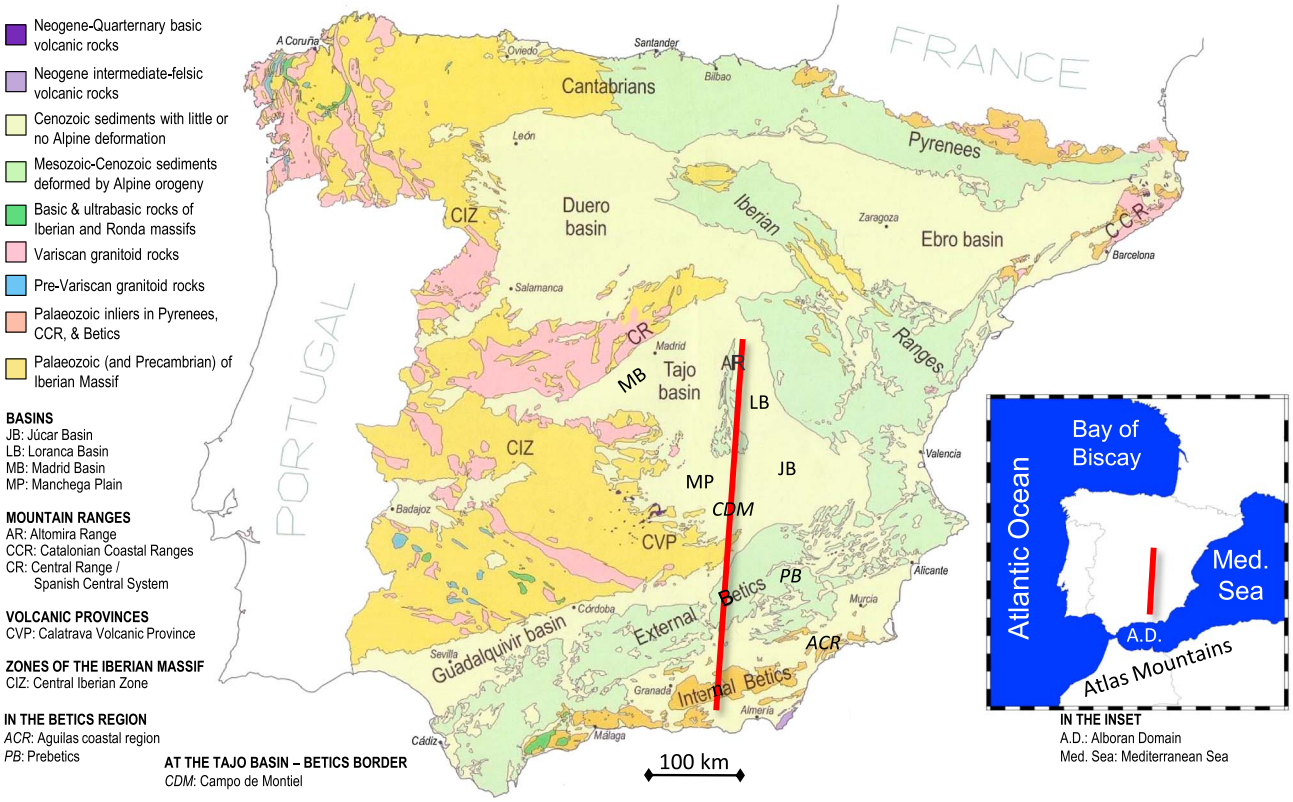

Figure 1. Geology of the Spanish part of the Iberian Peninsula displaying the main tectonic features and geological units of Spain; modified after *Gibbons and Moreno* [2002a]. The location of the PICASSO Phase 1 profile is indicated by the red line.

temperature, water content, or partial melt in the subsurface, putting strong constraints on the petrological setting and making MT a formidable tool for probing near-surface as well as deep-seated regions.

For this study, MT data were acquired in the Iberian Peninsula during the first phase of the multinational, multidisciplinary PICASSO (Program to Investigate the Convective Alboran Sea System Overturn) program, within which tectonic processes and internal structure of the western Mediterranean lithosphere and surrounding regions are being studied. The PICASSO project is part of the TOPO-EUROPE initiative (www.topo-europe.eu), with a related MT program that investigates structures within the Atlas Mountains named TopoMed [*Ledo et al.*, 2011], and within the western Mediterranean named AMELIE [*Evans et al.*, 2010]. During PICASSO Phase 1, MT recordings were carried out along an approximately 400 km long, north south oriented profile situated in the Spanish Tajo Basin and Betic Mountain Chain regions (Figure 1). In the Tajo Basin, comprising the northern half of the profile, a difference of approximately 70° is determined for the geoelectric strike directions of the crust (≈N41°W) compared to the lithospheric mantle (≈N29°E). The different strike directions are most likely related to the different tectonic events forming the approximately NW-SE stretching Pyrenees in the northeast of the peninsula and the approximately NE-SW stretching Betic Mountain Chain in the south of the peninsula.

2. Geological Setting

Due to the distinct geological contrast between the eastern and western Iberian Peninsula, these two parts are commonly referred to as *Alpine Spain* and *Variscan Spain* (sometimes referred to as *Hercynian Spain*), respectively. The former is dominated by young belts and Mesozoic and Cenozoic rocks that were deformed by Alpine orogeny, whereas the latter comprises Precambrian and Palaeozoic rocks with a relatively small overprint by Alpine deformation [e.g., *Alvaro et al.*, 1979; *Gibbons and Moreno*, 2002a; *de Vicente et al.*, 2007]. Remarkable events of Alpine orogeny in the western Iberian Peninsula are the deformation related to the Central System southern thrust [e.g., *de Vicente et al.*, 2007] and the extensive Bragança-Vilariça-Manteigas,

Messejana, and Verin-Régua-Penacova faults [e.g., *Cabral*, 1989; *Ribeiro et al.*, 1990; *Brum Ferreira*, 1991; *Andeweg*, 2002; *Rockwell et al.*, 2009].

Thorough descriptions of the Iberian Peninsula geology are given in, among others, *Gibbons and Moreno* [2002b, and references within], *Vera* [2004, and references within], and *Moratti and Chalouan* [2006, and references within]. Previous geophysical studies, in particular MT, have focused on the Pyrenees and the Betic Mountain Chain region with their Alpine Orogeny; see *Korja* [2007] for a summary of deep-probing MT investigations in the whole of Europe. The central Iberian Peninsula has mainly been the subject of near-surface research and has remained comparatively neglected in terms of deep-probing investigations. The focus of this study is on the crustal structure of the Tajo Basin located in the center of the Iberian Peninsula; later papers will discuss the PICASSO results pertinent to the Betic Mountain Chain.

2.1. Tajo Basin

The Tajo Basin (or Cuenca Basin, in English, also the Spanish *Tagus Basin*, not to be mistaken with the basin of the same name in Portugal) is bordered by basement uplifts; to the west by the Iberian Massif, to the north by the Spanish Central System (SCS, also *Central Range, CR*), to the east by the Iberian Range (also Iberian Chain), and to the south by the Betic Mountain Chain (Figure 1). Note that in some stratigraphical studies the Tajo Basin is referred to as the Madrid Basin, e.g., *Friend and Dabrio* [1996]. In this paper, following the nomenclature in *Gibbons and Moreno* [2002b], this basin is referred to as the Tajo Basin, with the Madrid Basin (or subbasin) located within the north western region of the Tajo Basin (cf. Figure 1, MB identifies the location of the Madrid Basin).

The Tajo Basin formed during the Anisian age (Middle Triassic) and subsequently widened until the Norian age (Late Triassic) due to the propagation of the Tethys Sea (which later became the Tethys Ocean) over the eastern margin of the Iberian plate [*López-Gómez et al.*, 2002]. Arising shallow marine carbonates drowned the NW-SE trending Palaeozoic high that originally separated the Tajo Basin from the northern regions of Iberia, resulting in a basin that is bounded to the NW by the Iberian Massif, opened eastward to the Tethys, and linked with the Betic basin to the south [*López-Gómez et al.*, 2002]. The Tajo Basin was again separated from the northern regions of Iberia (forming the Ebro and Duero Basins, Figure 1) during Oligocene-early Miocene Alpine convergence between Iberia, Europe, and Africa (Palaeogene-Neogene times) due to the resulting uplift of the Iberian Ranges [*Aurell et al.*, 2002; *López-Gómez et al.*, 2002; *Martín-Chivelet et al.*, 2002; *de Vicente et al.*, 2011]. Thereafter, the Tajo Basin became the locus of Tertiary sedimentation, establishing it as an intracratonic depocenter [*Alonso-Zarza et al.*, 2002; *Gutiérrez-Elorza et al.*, 2002]. It underwent little to no alpine deformation but later became subdivided due to the late Oligocene to early Miocene uplift of the *Altomira Range* (AR, Figure 1), a branch of the Iberian Range. The Altomira Range (*Sierra de Altomira* in Spanish literature) is a narrow, north-south trending, westward vergent fold-and-thrust belt [*de Vicente et al.*, 1996; *Alonso-Zarza et al.*, 2002; *Andeweg*, 2002]. In their work on modeling stress data, *Muñoz-Martín et al.* [1998] validated the hypothesis of *Muñoz-Martín et al.* [1994] that the Altomira Range was formed as a lateral extrusion of the Mesozoic cover from a region located to the west of the range. *Muñoz-Martín et al.* [1998] relate the stress fields involved in the orogeny of the Altomira Range to a superposition of the regional compressional stress field that originated from the tectonic settings of the Pyrenees and Betic Mountain Chain at that time. To the west and east of the Altomira range are located the Madrid Basin (MB, Figure 1) and the much smaller Loranca Basin (LB, Figure 1, also referred to as *Intermediate Depression* or *western sector of the Júcar Basin*), which comprise, together with the Manchega Plain (MP, Figure 1) to the south, the subbasins into which the Tajo Basin is commonly subdivided [*Alonso-Zarza et al.*, 2002; *Andeweg*, 2002; *Gibbons and Moreno*, 2002a; *Gutiérrez-Elorza et al.*, 2002] (Figure 1).

The *Loranca Basin* has been characterized as a foreland basin produced by a westward moving Iberian fold-and-thrust belt that some authors interpret as the front of the Pyrenean System [*Banks and Warburton*, 1991; *Gómez et al.*, 1996]. The Basin possesses a 1–1.4 km thick layer of Eocene to Quaternary sediments containing primarily sandstone, gravel, mudstones, limestone, gypsum, and lacustrine carbonates [*Gómez et al.*, 1996; *Torres et al.*, 1997; *Andeweg*, 2002]. The basin experienced a folding phase during the early Miocene, presumably due to the onset of the Betics-Iberian collision [*Muñoz-Martín et al.*, 1994; *Andeweg*, 2002]. The *Madrid Basin* (MB, Figure 1) is located in the north western region of the Tajo Basin and is drained by the Tajo River (English: Tagus River). The westernmost part of the Madrid basin, i.e., the Campo Arañuelo subbasin, has no sedimentary cover. To its south, the *Manchega Plain* (MP, Figure 1), representing the southern region of the Tajo Basin, comprises Quaternary aeolian sediments covering a substratum made up of the terraces of

the alluvial systems of the Guadiana and the Júcar rivers [*Rebollal and Pérez-González*, 2008]. Further south at the Tajo Basin border, the Campo de Montiel (CDM, Figure 1), a region of low-lying hills of carbonates, formed during Jurassic-Triassic times and may constitute the southernmost part of the Iberian Ranges adjacent to the Betic Mountain Chain [*Aurell et al.*, 2002; *Gutiérrez-Elorza et al.*, 2002]. Hence, the Jurassic strata of Iberian Range and Campo de Montiel are potentially connected below the Manchega Plain and the Júncar Basin forming the base of the overlying younger layers [*Aurell et al.*, 2002].

From previous seismic and thermal studies the subsurface below the Tajo Basin can be inferred to comprise sedimentary cover with a thickness of 1–3 km on top of three crustal layers, penetrating down to depths of 8–12 km, 23–25 km, and 30–33 km, respectively [*Banda et al.*, 1981; *Suriñach and Vegas*, 1988; *ILIHA DSS Group*, 1993; *Tejero and Ruiz*, 2002; *Julià and Mejía*, 2004; *Dáaz and Gallart*, 2009]. It has further been proposed, based on results of thermal modeling studies and transformation of seismic tomography data, that the thermal lithosphere-asthenosphere boundary (tLAB) is located at a depth of between 110 km and 130 km beneath the Tajo Basin [*Tejero and Ruiz*, 2002; *Artemieva*, 2006; *Tesauro et al.*, 2009a, 2009b].

The upper crustal layer is thought to be formed from crystalline rocks (quartzite or granite layer), and seismic and xenolith studies indicate that the middle and lower crust comprise felsic intrusives and granulites, respectively [*Banda et al.*, 1981; *Villaseca et al.*, 1999; *Tejero and Ruiz*, 2002]. A comprehensive discussion regarding the composition of the middle and lower crust of the Iberian Peninsula is given by *Villaseca et al.* [1999]. Since no seismic activity was recorded below the middle crust [*Instituto Geográfico Nacional, Seismic Information Service*, 2010], it is likely that the lower crust is an incompetent, ductile layer between the mantle and the overlying crustal layers.

Gravity data of the Iberian Peninsula, provided by the Spanish Instituto Geográficio National (IGN), were used, for example, by *Torné et al.* [2000] and *Gómez-Ortiz et al.* [2005] to investigate the crustal structures in this area.

Investigations of Neotectonic stress tensors in the SCS and the Madrid Basin [*de Vicente et al.*, 1996; *Andeweg et al.*, 1999] indicate average directions of largest horizontal shortening lying between N25°W and N50°W for the different geological times from Middle Miocene to the present day. A number of exposed faults, identified in the study of *de Vicente et al.* [1996], intersect the PICASSO Phase 1 MT profile, exhibiting a strike direction of approximately N45°W. Even though precise depth extent of these faults is presently unknown, they could provide a good approximation of the dominant geoelectric strike direction to be expected for shorter period MT data relevant to the Tajo Basin crust. Other subhorizontal material interfaces at crustal depths below the Tajo Basin, as deduced from lateral changes of seismic velocity, coincide with the borders of the Betic Mountain Chain and the Iberian Range [*Villaseñor et al.*, 2007] (Figure 2). The respective ENE-WSW and NW-SE orientation of these interfaces indicate different geological strike directions, and thus infer different geoelectric strike directions, for the northern and southern parts of the MT profile. Furthermore, a low velocity feature, occurring slightly north of the Betic Mountain Chain, is suggested to extend down to at least 300 km, whereas the anomaly associated with the Iberian Range is not observed at depths greater than 53 km in the seismic tomography models of *Bijwaard et al.* [1998] and *Amaru et al.* [2008] (see *Amaru* [2007], for figures of these models). Hence, it is likely that the geoelectric strike direction in the Tajo Basin below the MT profile will also change with depth.

The seismic tomography studies by, among others, *Bijwaard et al.* [1998], *Villaseñor et al.* [2007], and *Amaru et al.* [2008] define low velocity structures at crustal depths beneath the Betic Mountain Chain and Alboran Sea, in the middle and lower crust beneath the Campo de Montiel region and an extensive low-velocity region located approximately 50 km to 350 km beneath the Tajo Basin (Figure 3). Different scenarios could explain such decreases of velocity, e.g., increased temperature, different chemistry, and the presence of partial melt or fluids [e.g., *Sato et al.*, 1989; *Goes et al.*, 2000]. The anomaly beneath the western Mediterranean Sea (labeled "a" in Figure 3) is potentially due to subduction or delamination of lithospheric material, being replaced by warmer and therefore less dense mantle material [e.g., *Torres-Roldan et al.*, 1986; *Platt and Vissers*, 1989; *Seber et al.*, 1996; *Calvert et al.*, 2000; *Gutscher et al.*, 2002; *Amaru*, 2007]. The descending lithospheric material is most likely represented by feature "b" in Figure 3, i.e., the observed relatively high-velocity region in the asthenosphere beneath Alboran Sea and Betic Mountain Chain. A slab subducting beneath the Alboran Sea and Betic Mountain Chain has been modeled in seismic tomography studies of *Bijwaard et al.* [1998], *Spakman and Wortel* [2004], and *Amaru* [2007]. Beneath the Tajo Basin, extending closest to the surface beneath its southern boundary, is the northward dipping, low-velocity region labeled

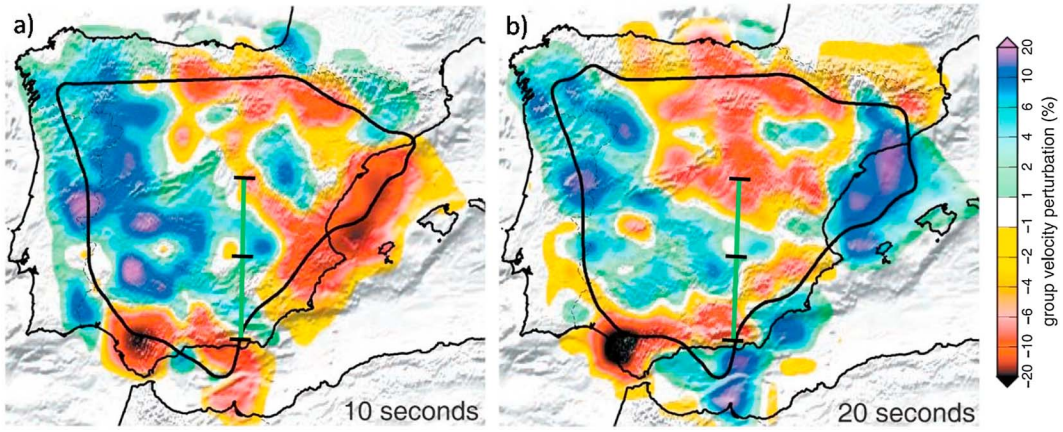

Figure 2. Group velocity maps of the Iberian Peninsula subsurface, obtained from ambient noise tomography using Rayleigh waves at periods of (a) 10 s and (b) 20 s, related to structures of the upper 10 km and between 15 km and 30 km, respectively. Thick contour lines indicate the region in which features with a lateral extent greater than 100 km are well resolved; from *Villaseñor et al.* [2007]. Green lines denote the location of the PICASSO Phase 1 MT profile, with black ticks indicating the limits of the profile and the boundary between Tajo Basin (to the north) and Betic Mountain Chain (to the south).

"c" in Figure 3. This deep-seated anomaly is in agreement with structures identified in previous models by *Hoernle et al.* [1995] and *Bijwaard et al.* [1998], who both defined a structure of similar location and depth extent with an ENE-WSW orientation. *Hoernle et al.* [1995] interpreted the low-velocity region to be a "relatively hot (possibly volatile-enriched) region of mantle upwelling." According to its location, this anomaly could potentially be related to the Betic Mountain Chain-Iberian Peninsula collision in Miocene times or to the subducting lithosphere beneath Alboran Sea and Betic Mountain Chain. However, its vast depth extent is somewhat puzzling. Hence, at the current stage of knowledge, the interpretation by *Hoernle et al.* [1995] cannot be refuted.

The Calatrava Volcanic Province (CVP, Figure 1), one of the four main provinces of Cenozoic volcanism in Iberia, is situated in the southwestern region of the Tajo Basin around the city of Ciudad Real, located approximately 100 km to the west of the profile (Figures 1 and 4). Two different sources have been determined for the CVP rocks by *López-Ruiz et al.* [1993] and *Cebriá and López-Ruiz* [1995, 1996] based on geochemical composition; namely, either ^{87}Sr-enriched–^{143}Nd-depleted continental lithospheric mantle or ^{87}Sr-depleted–^{143}Nd-enriched sublithospheric source relative to primitive mantle. The authors relate the

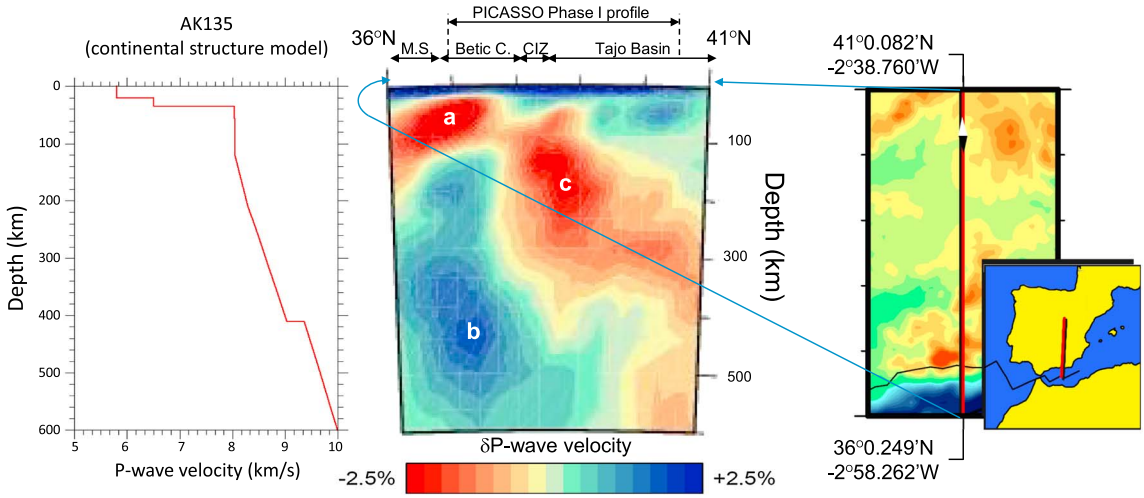

Figure 3. (left) *P* wave velocity relative to the AK135 reference model [*Kennett et al.*, 1995] for a transect coinciding with the (right) PICASSO Phase 1 profile, extracted from a global travel time tomography model [*Amaru*, 2007]; Betic C.: Betic Mountain Chain, CIZ: Central Iberian Zones, M.S.: Mediterranean Sea; see text for details.

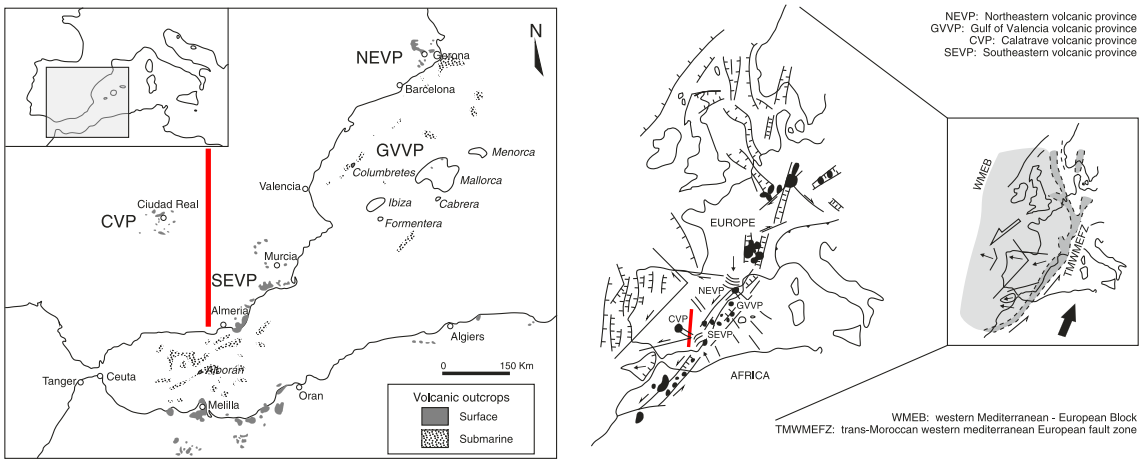

Figure 4. (left) Cenozoic volcanic provinces in the SE Iberian Peninsula and NW Africa. (right) Tectonomagmatic scenario for the latest Miocene to present alkaline basaltic volcanism in western Europe; modified after *López-Ruiz et al.* [2002]. The tectonomagmatic scenario involves a NW-SE connection between the trans-Moroccan, western Mediterranean European (TMWME) fault zone and the Calatrava volcanic province (CVP) intersecting the PICASSO Phase 1 profile (indicated by the red line) in the area of the Campo de Montiel region.

former to potassic volcanism during Miocene times (6.4–7.3 Ma) with olivine leucitites, whereas the latter is concluded to have formed the alkali basalts during Pleistocene and Pliocene times (1.5–5 Ma). Age determination of the two volcanic intervals were based on K-Ar ratio analyses by *Ancochea et al.* [1979] and *Bonadonna and Villa* [1986]. For the basaltic suite, *Cebriá and López-Ruiz* [1995, 1996] determined the degree of partial melting of between 5% and 17% using quantitative trace element modeling, whereas for the olivine leucitites, a relatively low degree of partial melting (≈4%) was inferred. Based on lava composition and geological characteristics of the related regions, a two-stage process was proposed by *López-Ruiz et al.* [1993] (later corroborated by *Cebriá and López-Ruiz* [1995] and *López-Ruiz et al.* [2002]). The first (Mesozoic) stage comprised melting of the lithospheric mantle by a mantle diapir, resulting in the olivine leucitite volcanism and causing general weakening of the crust. During the second (Pliocene) stage, tectonic indentation in the eastern Betic Mountain Chain (SE border of the Iberian Peninsula) [*Doblas et al.*, 1991] led to feeding of asthenospheric material in a northwestern direction, causing the basaltic volcanism in the CVP.

CVP lavas of the secondary process may have been transported through a lithospheric fault network that was formed by extensional tectonics during late Miocene times [*López-Ruiz et al.*, 1993, 2002]; a hypothesis that is supported by predominant NW-SE trends of emission vents in the CVP [*Ancochea and Brandle*, 1982]. A connection between the CVP and the eastern Betic Mountain Chain region is inferred by *Cebriá and López-Ruiz* [1995] and *López-Ruiz et al.* [2002], based on the similarity of the basalt composition of the CVP rocks with the extensive trans-Moroccan, western Mediterranean, European (TMWME) reservoir that is the cause of volcanic events across the whole of Europe and the eastern Atlantic [*Wilson and Downes*, 1991; *Cebriá and Wilson*, 1995; *Hoernle et al.*, 1995] (cf. Figure 4). The indentation event in the eastern Betic Mountain Chain, which is thought to have initiated the second CVP event, is in agreement with the convex-to-the-NW arc-shaped geometry of the Prebetics (NE region of the External Betics) and the Aguilas coastal region (SE edge of the Iberian Peninsula), as well as the uplift in the Campo de Montiel region (*Ruidera uplift*) [*López-Ruiz et al.*, 1993]. The PICASSO Phase 1 MT investigation provides additional information about the nature of the second stage since, in the case of the Betic Mountain Chain indentation source proposed by *Cebriá and López-Ruiz* [1995] and *López-Ruiz et al.* [2002], the course of the lava transport would intersect the MT profile in the area of the Campo de Montiel region.

2.2. Iberian Massif

To the west of the Tajo Basin, accounting for the majority of the western region of the Iberian Peninsula, outcrops the *Iberian Massif*, constituting the oldest part of the European Variscan orogeny formed during Middle Devonian-Early Permian times as a consequence of the collision between Laurentia and Gondwana [e.g., *Colmenero et al.*, 2002; *Gibbons and Moreno*, 2002a]. The Iberian Massif was above sea level during pre-Cenozoic times and had a planar and low relief [*Stapel*, 1999], but was subsequently deformed by various Cenozoic tectonic events resulting in an arcuate geometry [e.g., *Andeweg*, 2002; *Colmenero et al.*, 2002;

Gibbons and Moreno, 2002a, and references within]. The Iberian Massif consists mainly of igneous and metamorphic rocks and has commonly been divided into six zones or domains with the *Central-Iberian Zone* (formed by Precambrian and Paleozoic rocks) bordering the Tajo Basin to the west and southwest as well as to the northwest as part of the SCS [*Colmenero et al.*, 2002; *Tejero and Ruiz*, 2002; *Valladares et al.*, 2002] (Figure 1). The location and shape of the interface between the Variscan rocks of the Iberian Massif and the Jurassic-Triassic rocks forming the Iberian Range is presently unclear for the region below the Tajo Basin. However, since the Altomira Range is part of the Iberian Range, the interface is most likely to be found to the south and west of the Altomira Range, below the Madrid Basin and Manchega Plain. Thus, crustal structures derived from MT stations located in the Loranca Basin and the Manchega Plain yield further information about the Iberian Massif-Alpine Spain interface in this region.

3. The Magnetotelluric Method

MT has been successfully applied in numerous tectonic studies (recently reviewed by *Unsworth* [2010], *Weckmann* [2012], and *Selway* [2013]), and here only a very brief general overview about basic MT principles is given; for more detailed discussion of theoretical aspects of the MT methods, the interested reader is referred to standard literature [e.g., *Schmucker*, 1973; *Vozoff*, 1987; *Berdichevsky*, 1999; *Simpson and Bahr*, 2005; *Becken et al.*, 2008; *Berdichevsky et al.*, 2009] and the new book by *Chave and Jones* [2012], as well as the review papers from the biennial IAGA EM Induction Workshops. In MT, the depth of investigation is directly dependent on the period of the utilized electromagnetic waves and the resistivity of the subsurface, so penetration to all depths is assured, albeit with broader and broader resolution kernels. MT is superior to potential field methods like gravity, magnetics, or thermal modeling that are inherently nonunique and require a range of assumptions to be made regarding values and distribution of related parameters within the Earth. There exists a uniqueness theorem for the MT impedance in some circumstances [*Bailey*, 1970], so, unlike potential field methods, MT is not inherently nonunique. MT is steadily gaining in popularity among geoscientists since its development by *Rikitake* [1948], *Tikhonov* [1950], and *Cagniard* [1953] in the middle of the last century, and has been used to study various aspects in almost all regions of the world.

For the MT method, natural electromagnetic (EM) field time variations in typically the period range 10^{-3}–10^{4} s (although much shorter and much longer periods are used) are used to deduce the distribution of electric resistivity ρ (or its inverse, electrical conductivity σ) within the Earth and, through that, infer the geometries of the geological setting of the subsurface. Deep crustal and mantle probing EM field variations at periods greater than 0.1 s (frequencies lower than 10 Hz) originate from interaction of electrical charged particles radiated from the Sun (the solar wind) with the Earth's ionosphere and magnetosphere. Upper crustal information is obtained from EM field variations from distant lightning storms that generate energy at frequencies greater than 8 Hz (Schumann resonance). Time variations of the electric (E) and magnetic (H) field components are recorded at the Earth's surface by measuring potential field differences between two electric sensors (nonpolarizable electrodes) and magnetic induction in magnetic sensors, respectively. Since induction depths of EM waves are period dependent, information about different depth regions within the subsurface is obtained using E and H field relationships at respective periods in exactly an analogous manner to longer-period seismic surface waves penetrating deeper into the Earth. Time series of the E and H field components are almost always transformed from the time domain into the frequency domain using Fourier transformation, and EM field relations are expressed using the electric impedance tensor **Z**(T), which can be written in compact form as

$$\vec{E}(T) = \mathbf{Z}(T) \cdot \vec{H}(T) \tag{1}$$

$$\Leftrightarrow \begin{pmatrix} E_x(T) \\ E_y(T) \end{pmatrix} = \begin{pmatrix} Z_{xx}(T) & Z_{xy}(T) \\ Z_{yx}(T) & Z_{yy}(T) \end{pmatrix} \cdot \begin{pmatrix} H_x(T) \\ H_y(T) \end{pmatrix}. \tag{2}$$

where E_x, E_y, H_x, and H_y denote respective horizontal components of electric and magnetizing fields in the frequency domain related to the x and y direction in a given coordinate system, and T indicates dependency on the period of the EM field. The complex impedance tensor elements Z_{ij} are commonly expressed using the so-called apparent resistivity

$$\rho_{a_{ij}}(T) = \frac{1}{\mu\omega} \left| Z_{ij}(T) \right|^2 \tag{3}$$

and impedance phase

$$\phi_{ij}(T) = \arctan\left(\frac{\Im(Z_{ij}(T))}{\Re(Z_{ij}(T))}\right) \tag{4}$$

with $i, j \in [x, y]$.

The complexity of the impedance tensor **Z** can be reduced when the subsurface is one-dimensional (1-D), i.e., it comprises only vertical changes of electrical conductivity. In that case, diagonal elements of **Z** are equal to zero and off-diagonal elements exhibit the same amplitude but different signs, i.e., $Z_{yx} = -Z_{xy}$ [e.g., *Vozoff*, 1987]. Different signs of the 1-D off-diagonal impedance tensor elements are due to the use of right-hand and left-hand coordinate systems for Z_{xy} and Z_{yx} elements, respectively:

$$\mathbf{Z}_{1D} = \begin{pmatrix} 0 & Z_{xy}(T) \\ -Z_{xy}(T) & 0 \end{pmatrix}. \tag{5}$$

In the two-dimensional (2-D) case, i.e., when the subsurface comprises lateral conductivity interfaces in only one direction (with an arbitrary number of vertical conductivity changes), the coordinate system used for recording can be rotated by an angle Θ to fit the interface direction using a transformation tensor

$$\mathbf{R} = \begin{pmatrix} \cos(\Theta) & \sin(\Theta) \\ -\sin(\Theta) & \cos(\Theta) \end{pmatrix}. \tag{6}$$

For the case that the rotated coordinate system and lateral conductivity interface direction are perfectly aligned, the impedance tensor reduces to

$$\mathbf{Z}_{2D} = \begin{pmatrix} 0 & Z_{xy}(T) \\ Z_{yx}(T) & 0 \end{pmatrix}, \tag{7}$$

and equation (1) to

$$E_x(T) = Z_{xy}(T)H_y(T) \tag{8}$$

$$E_y(T) = Z_{yx}(T)H_x(T). \tag{9}$$

In 2-D MT investigation, it is common practice to define the *x* axis parallel to, and the *y* axis orthogonal to, the strike direction of the lateral electric resistivity interfaces, with the latter determining the direction of the profile for modeling. Elements Z_{xy} and Z_{yx}, therefore, comprise data of the electric component parallel and the magnetic component orthogonal, to the resistivity interface, and vice versa. In the 2-D case, Z_{xy} and Z_{yx} are commonly referred to as transverse electric (TE) and transverse magnetic (TM) mode response data, respectively; less commonly used older terms can be found in the literature, with E polarization or E parallel for the TE mode and H polarization or B polarization or E perpendicular for the TM mode.

As shown in the previous paragraphs, for the ideal 1-D and 2-D cases, the number of free parameters of **Z** per period can be reduced from eight to two and four, respectively (each impedance tensor elements has a real and imaginary component). Such a reduction in dimensionality significantly reduces computational expense and time of MT modeling; however, respective reductions have to be justified. In most cases, the investigator aims to identify a regional 2-D subsurface model that fits the recorded data within given error bounds.

A commonly used tool in MT investigations to determine suitable data for a 2-D model is the `strike` program by *McNeice and Jones* [2001], based on the theory by *Groom and Bailey* [1989]. In their classical paper, *Groom and Bailey* [1989] use nine parameters to decompose the recorded impedance tensor into contributions of a regional 2-D structure (equation (7)) with a given strike, and a series of local sources, namely, gain, twist, shear, and anisotropy, due to galvanic distortions of the electric field. A key element is the orientation of the vertical resistivity interface, the so-called geoelectric strike direction. Besides the fact that a correctly identified strike direction permits reduction of the adopted dimensionality of the impedance tensor, the strike direction can, by itself, yield valuable insight about geological structures of the subsurface, e.g., when correlated with lithological variations at depth that originate from present or past tectonic processes.

An example of this is the work of *Hamilton et al.* [2006], who related geoelectric strike directions to tectonic features. The `strike` program derives the regional $\mathbf{Z}_{2D}$, the strike direction, and the four local distorting sources, and, in particular, evaluates the suitability of the *Groom and Bailey* [1989] distortion model on a statistical basis. Hence, the program determines whether the assumption of a subsurface with a regional 2-D geoelectric strike is valid within the given error bounds of the data themselves.

In addition to the relation between horizontal $\vec{E}$ and $\vec{H}$ fields described in previous paragraphs, the relation between horizontal and vertical H fields (H_x and H_y to H_z, respectively) can be used to derive subsurface structures. The vertical magnetic transfer function $\vec{T} = (T_x, T_y)$, also referred to as *Tipper*, is defined as

$$H_z(f) = \vec{T}(T) \cdot \vec{H}(T). \tag{10}$$

For the case of a 2-D subsurface and adequate rotation of the coordinate system, equation (10) reduces to

$$H_z(f) = T_y(T) \cdot H_y(T). \tag{11}$$

where the *y* axis is defined parallel to the conductivity interface [e.g., *Vozoff*, 1986]. The magnetic transfer function can be displayed using so-called induction arrows, with arrows pointing either away from (Wiese convention [*Wiese*, 1962]) or toward (Parkinson convention [*Parkinson*, 1959]) conductive regions, ignoring the pathological case that occurs at high frequencies above the skin depth to the structure when the arrows point in the opposite directions [*Jones*, 1986]. For the true 2-D case, the real and imaginary parts of T_y are a Hilbert transform pair; thus, at the maximum magnitude in the real induction vector, the imaginary induction arrow equals zero. Typically, only the real induction arrows are considered qualitatively, but both the real and imaginary parts of the Tipper are modeled during inversion.

4. Data Acquisition and Processing

4.1. Profile Location

In October and November 2007, MT data were acquired along an approximately 400 km long, north-south oriented profile from its northern end some around 100 km east of Madrid to the city of Almeria near the Mediterranean Sea, crossing the Tajo Basin and the Betic Mountain Chain (cf. Figures 1 and 5). The north-south orientation of the profile was chosen in order to cross the main geological feature being studied, i.e., the Tajo Basin, across its maximum extent and also to allow for continuation of the profile across the Mediterranean Sea into Morocco on the southern side of the Mediterranean. Subsequent fieldwork campaigns have been conducted as part of the PICASSO Phase 2, TopoMed, and AMELIE projects in Morocco and the Alboran Sea [e.g., *Evans et al.*, 2010; *Kiyan et al.*, 2011; *Ledo et al.*, 2011]. As well as being informative in their own right about the nature of the lithosphere of the central Iberian Peninsula, data from the PICASSO Phase 1 project supports investigations in these subsequent projects regarding the nature of the putative anomaly beneath the Alboran Domain [e.g., *Platt and Vissers*, 1989; *Seber et al.*, 1996; *Calvert et al.*, 2000] and the complex plate tectonic processes involved in the continental collision between Africa and Europe [e.g., *Andeweg et al.*, 1999; *de Vicente and Vegas*, 2009]. Those issues are not addressed here however.

The locations of MT stations were chosen to avoid sources of electromagnetic (EM) noise, like highly populated areas and the electric train network, as much as possible. Along the profile, data were successfully recorded at 25 locations using Phoenix Geophysics broadband MTU-V5A systems and Lviv long-period LEMI-417 systems, with interstation separation close to 20 km. Additional infill broadband recordings were conducted along certain parts of the profile, reducing the station spacing to approximately 10 km in those localities, in order to increase the resolution in the respective regions.

4.2. Analysis of Collected Data

After field layout correction and standard preprocessing, the time series data were processed using a multitude of different remote reference, robust processing algorithms, among which the algorithms by *Egbert* [1997] and *Smirnov* [2003] yielded the most superior results in terms of usable period range and lowest scatter of the impedance estimates for the broadband and long-period data, respectively. Signal-to-noise ratio of the data set was, in general, lower than typical compared to normal MT data due to a combination of low signal and high noise; the former being the elongated phase of exceptional low solar activity at the end of Solar Cycle 23 during the recording time, and the latter being the extensive electrical infrastructure of Spain. In particular, electric noise of the DC railway line, intersecting the MT profile between stations pic013

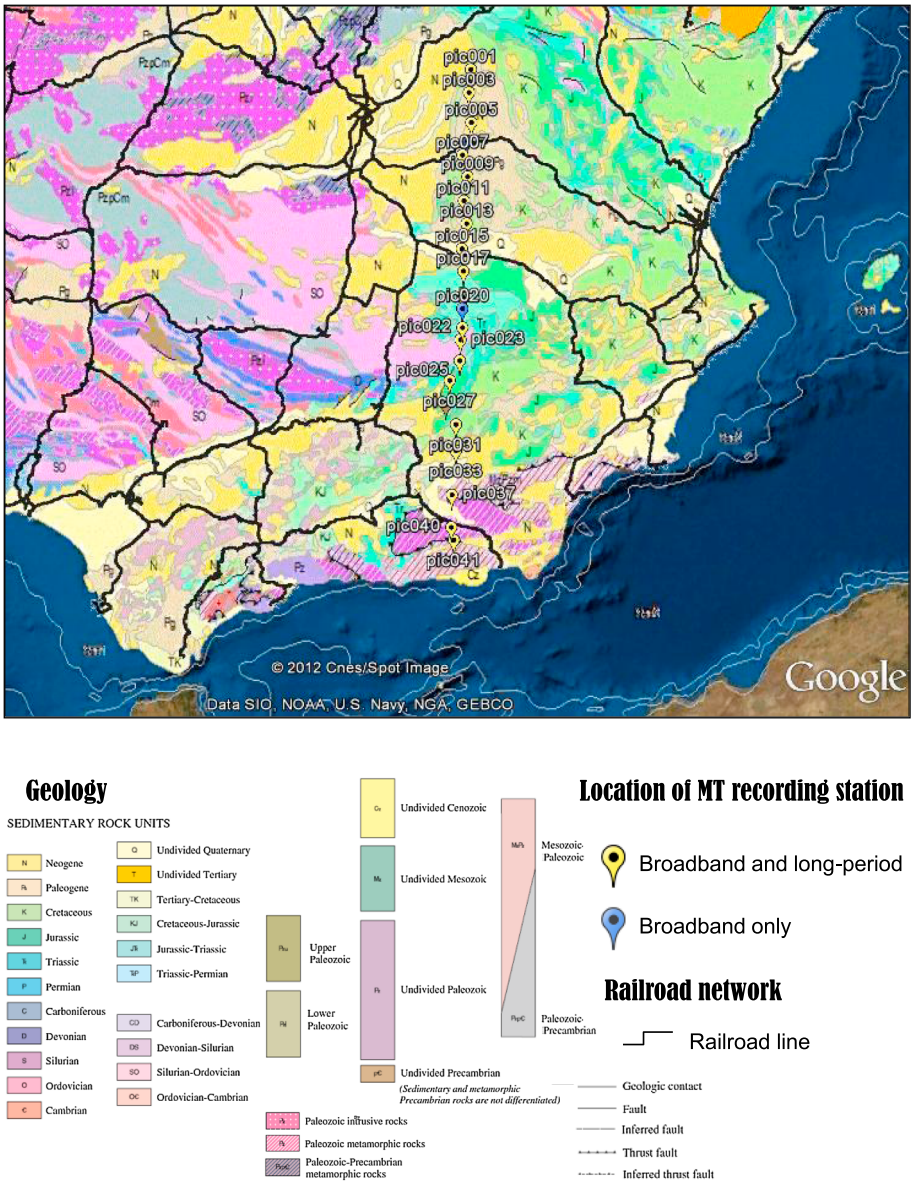

Figure 5. Location of PICASSO Phase 1 recording stations, together with the Spanish DC railroad network in the study area (black lines) on top of the surface geological map of Spain from the EnVision map of the *USGS Energy Resources Program* [2010]. Pins indicate the location of magnetotelluric recordings, with colors denoting sites where only broadband systems (blue pins) and both broadband and long-period systems (yellow pins) are used.

and pic015 (Figure 5), had severe influence on the response data, shown by phase values of approximately 0 degrees that are indicative of the site being in the near-field of an EM source. Disturbance by this electric noise resulted in complete deletion of long-period data from stations pic013 and pic015 and truncation of the responses for stations pic011, pic017, and pic019 at 1500 s on the basis of D^+ tests [*Parker*, 1980; *Parker and Whaler*, 1981; *Parker*, 1982]. In addition, the long-period data of station pic022 had to be rejected, and responses of stations pic023 and pic027 were truncated at 900 s, in order to remove data corrupted by electromagnetic noise. Subsequent to the separate processing of broadband and long-period data, responses were merged for stations where both types were available. As both systems used exactly the same electrode array, the two sets of responses were within each other's error bounds at overlap periods, and no shifting of the apparent resistivity curves, to compensate for different static shift effects [*Jones*, 1988], was required.

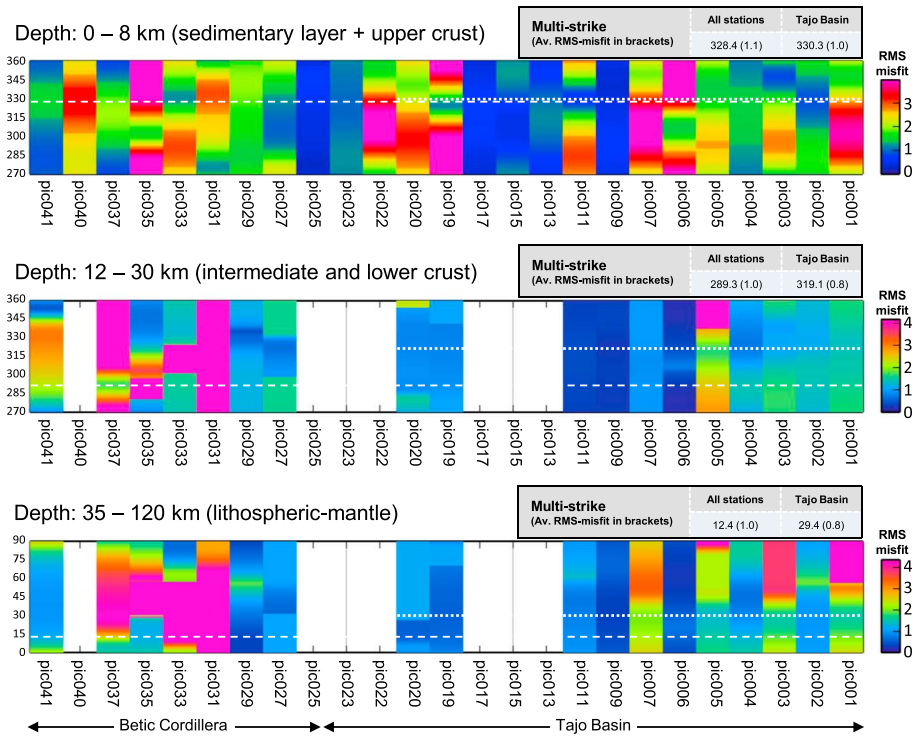

Figure 6. RMS misfit for different geoelectric strike directions (color coded with warm colors indicating high misfits) applied to data from magnetotelluric (MT) stations recorded during PICASSO Phase 1, using data in the Niblett-Bostick depth ranges 1–8 km (sedimentary layer and upper crust), 12–30 km (middle and lower crust), and 35–120 km (lithospheric mantle) (for more details, see *Schmoldt* [2011]). Empty spaces are due to lack of suitable data for this depth range at the respective station. Also shown in the top right corner, as well as indicated by white lines, in the plots for each depth region are the optimal common geoelectric strike directions for the whole PICASSO Phase 1 profile (dashed lines) and for stations in the Tajo Basin (dotted lines) calculated using the multisite, multifrequency approach of the program `strike` by *McNeice and Jones* [2001]. The 90° ambiguity of MT strike determination [e.g., *Groom and Bailey*, 1989] is resolved using the direction of induction arrows and results of seismic studies (Figure 2).

4.3. Geoelectric Strike Estimation

Determining whether a regional 2-D approximation is justified, and, if found to be true, subsequent identification of the geoelectric 2-D strike direction are major elements of MT impedance tensor analysis as it affects the decomposition of EM fields into the regional TM and TE mode contributions. In this work, the multisite, multifrequency approach of the `strike` algorithm [*McNeice and Jones*, 2001] was used for analysis of the MT impedance response estimates. Optimal strike direction and average RMS misfit for models of regional 2-D structures and local distortion were calculated for groups of stations and depth ranges, with the latter derived using the Niblett-Bostick depth approximation [*Niblett and Sayn-Wittgenstein*, 1960; *Bostick*, 1977; *Jones*, 1983a] for the rotational invariant arithmetic average of the off-diagonal elements (also referred to as the *Berdichevsky average*) [*Berdichevsky and Dmitriev*, 1976]. Example of this approach are shown in *Miensopust et al.* [2011] and *Adetunji et al.* [2014]. A relative impedance error floor of 3.5% was used during the application of the `strike` algorithm, resulting in an error floor of 2.0° for the phase and 7.12% for the apparent resistivity.

Thorough investigation of the geoelectric strike direction beneath the MT profile resulted in the following conclusions (cf. Figures 6 and 7), where the thicknesses of the layers were defined according to results of previous seismic and thermal modeling studies [e.g., *Banda et al.*, 1981; *ILIHA DSS Group*, 1993; *Tejero and Ruiz*, 2002; *Julià and Mejía*, 2004; *Artemieva*, 2006; *Tesauro et al.*, 2009b]. Figure 6 shows the variation with strike angle for each individual site for the three depth subsets, color coded so that blue is acceptable, and red is not acceptable. Figure 7 shows the statistics at each geoelectric strike angle, from 0° to 90° at 5° increments, in box-and-whisper quartile plots for each depth range (A, B, and C) and for each of the two subsets, i.e., data from all stations (top plot) and Tajo Basin only stations (bottom plot). Also shown are the averages for each strike direction (red dots and lines). The multisite, multidepth solutions from the

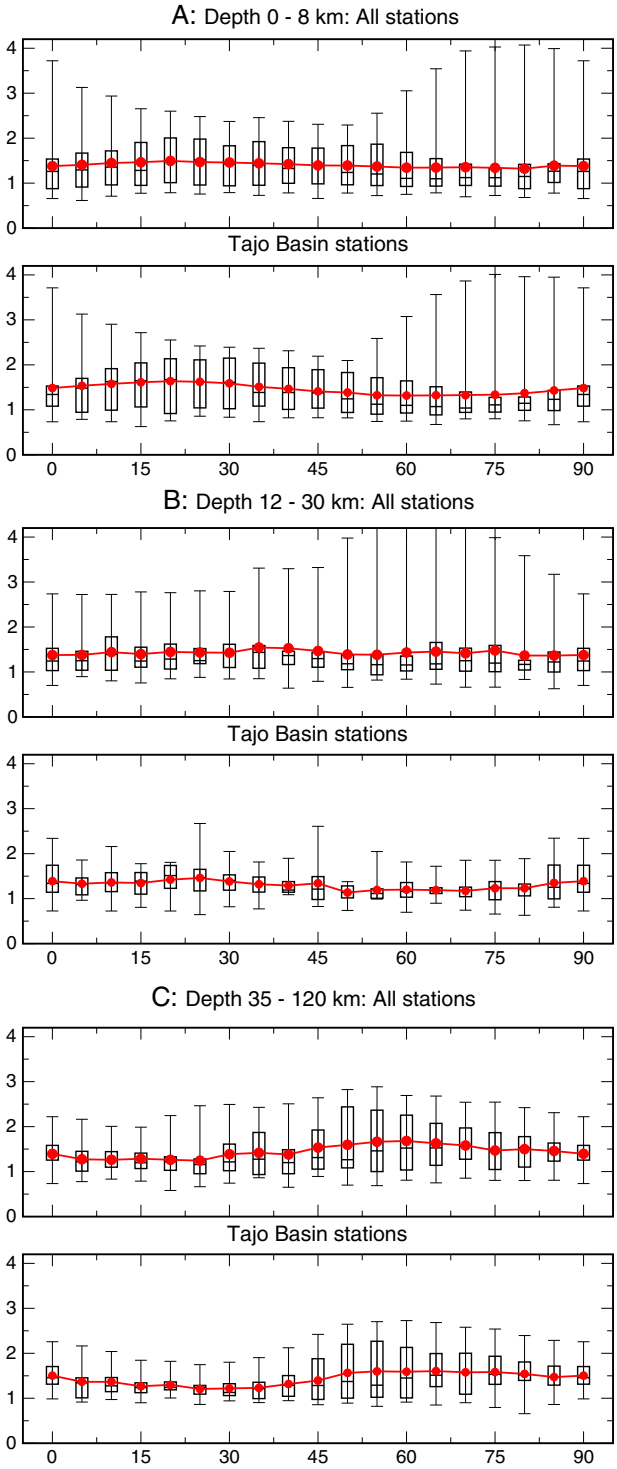

Figure 7. Statistics of station RMS misfits for different geoelectric strike directions applied to data from magnetotelluric (MT) stations recorded during PICASSO Phase 1, using data in the Niblett-Bostick depth ranges (a) 1–8 km (sedimentary layer and upper crust), (b) 12–30 km (middle and lower crust), and (c) 35–120 km (lithospheric mantle). The same sites are included in each subset as shown in Figure 6. The box-and-whisker plots show the ranges of the individual RMS misfits in the given depth ranges for each 5° in the range 0°–90°. The red dots and lines show the averages for each depth and sites subset.

McNeice and Jones [2001] code for each of the three depths and each of the two subsets are listed in Figure 6. These solutions are verified by the detailed statistics in Figure 7, with the crustal depths (Figures 7a and 7b) exhibiting a preferred direction of around 60° (i.e., 330°), and the lithospheric mantle depth (Figure 7c) exhibiting a preferred direction of around 30° (i.e., 300°).

1. Strike characteristics differ between the southern region of the profile associated with the Betic Mountain Chain and the northern region associated with the Tajo Basin. The Betic Mountain Chain exhibits highly complex subsurface structures for the whole depth range, for which no distinct or predominant geoelectric strike direction can be identified, whereas for the Tajo Basin a common geoelectric strike direction can be found for the majority of the different depth layers.
2. Layers in the Tajo Basin subsurface can be grouped into two bands: crustal layers with a geoelectric strike direction dominated by structures of the intermediate and lower crust, i.e., N40.9°W (N319.1°E in Figure 6); and mantle layers with a geoelectric strike direction of N29.4°E, associated with the lithospheric mantle. In particular, although the curves of the average RMSes with rotation angle (Figure 7) are rather flat, but nevertheless they do show minima in the directions derived from the multisite, multidepth analyses, more importantly are the other statistics with rotation angle, i.e., the ranges, the medians, and the inner quartiles (Q2 and Q3). All of these verify the salient point that the crust and mantle have very different geoelectric strike directions.
3. Derived significant oblique strike directions between the crust and mantle are in agreement with the results of seismic tomography studies for the same region, determining changes of seismic velocity along a NW-SE oriented interface at crustal depth and a NNE-SSW oriented interface at mantle depths (cf. section 2.1).
4. The determined geoelectric strike direction at mantle depths is not in agreement with derived plate motion of

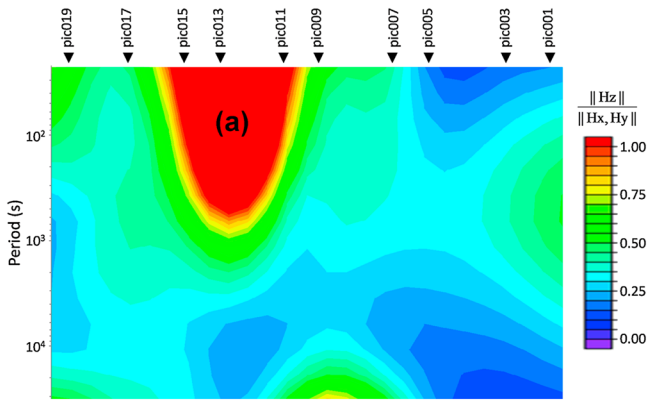

Figure 8. Magnitude of the magnetic transfer function for the Tajo Basin subsurface; see text for details. The interested reader will find a plot of the corresponding induction arrows in Figure 9.15 of *Schmoldt* [2011].

Eurasia (at Longitude: 3°W, Latitude: 40°N), i.e., N50.6°E (2.5 cm/a) [*Argus and Gordon*, 1991] and N50.5°E (2.4 cm/a) [*De Mets et al.*, 1994]. It is therefore unlikely that the mantle geoelectric strike direction originates from processes in connection with modern day plate motion. Thus, it is unlikely that effects of anisotropic structures, caused by lattice preferred orientation from drag along alignment at the LAB, are mistaken for 2-D structural strike [e.g., *Heise and Pous*, 2001; *Simpson*, 2001; *Bahr and Simpson*, 2002; *Hamilton et al.*, 2006; *Pek and Santos*, 2006; *Poe et al.*, 2010].

Oblique geoelectric strike directions for different subsurface regions are a known problem in MT investigation and have previously been reported by, among others, *Marquis et al.* [1995], *Eaton et al.* [2004], *Wu et al.* [2005], *Spratt et al.* [2009], and *Miensopust et al.* [2011]. Crustal structures can usually be determined by confining the modeled period range to crustal penetration depths; however, recovery of mantle structures is more challenging. No straightforward solution is currently known for the problem of deriving mantle structures for subsurfaces with significantly oblique strike directions, although *Schmoldt* [2011] and *Schmoldt and Jones* [2013] discuss approximate 1-D and 2-D modeling approaches using anisotropic techniques.

Due to the significantly oblique geoelectric strike directions of the Tajo Basin crust (N40.9°W) and mantle (N29.4°E), this study is focused on crustal structures only; features inferred at mantle depth are rendered inconclusive and are not included in this interpretation. Decomposition of the impedance tensor for each station into TE mode, TM mode, and distortion effects was carried out for the crustal strike direction of N40.9°W using the `strike` program for the Niblett-Bostick depth range of 0–30 km. Uncertainty levels for the TE and TM modes of each data set were determined on a statistical basis using a bootstrap approach assuming Gaussian distributions of the impedance elements with their variances as given by their sample variances. These estimates and their error estimates are used in the following.

4.4. Vertical Magnetic Transfer Function Estimates

Vertical magnetic transfer function response estimates were derived with the algorithm of *Smirnov* [2003], and the results reveal a significant distortion of magnetic data in the area around stations pic011, pic013, and pic015, indicated by a transfer function magnitude of greater than 1 (feature labeled "a" in Figure 8). For most cases, a magnitude greater than 1 is unlikely as this implies that $||H_z|| > ||H_y||$, requiring that the strength of the secondary field is greater than the strength of the primary field. In the late 1960s and 1970s, this was thought to be physically impossible and attributed to notorious "current channeling" [e.g., *Camfield et al.*, 1971], but it was shown to be possible for extremely strong conductors of large length extent [*Jones*, 1983b], such as the North American Central Plains conductivity anomaly (NACP) [see, e.g., *Jones et al.*, 2005]. In this case, however, no such strong conductor exists, and the effect is due to noise contributions in the near field of an external source, namely, the DC train line. The interpolated area of distortion has an approximately parabolic shape with its vertex beneath station pic013, at periods of approximately 10^3 s. The area of distortion widens at shorter periods, extending to the regions in-between stations pic009 and pic011 and stations pic015 and pic017 at periods around 10 s. The center of the anomalous area coincides with the intersection of the MT profile with a DC railway line at the surface (cf. Figure 5).

In our case, given the potential for distortion of the vertical magnetic transfer function estimates, we only use these data in a qualitative manner, both to examine the likely region affected by distortion and also to indicate possible 3-D effects.

4.5. Data Acquisition and Processing Conclusions

We conclude the data acquisition and processing section by remarking that we have chosen in this paper not to follow what is generally routine in MT papers by displaying the raw or decomposed MT responses, either as copious apparent resistivity and phase curves or in pseudosection format (apart from the along-profile vertical field magnetic transfer function shown in Figure 8). We consider that the vast majority of readers wish to see our models and the fit of our models to our data to assess the veracity of our models, thus, we present data misfit plots only. The interested reader will find all of the data plotted in the PhD thesis of J.-P. Schmoldt [*Schmoldt*, 2011], which is available online through MTNet (www.mtnet.info).

5. Inversion

Due to the highly complex nature of the Betic Mountain Chain and the circumstance that extensive MT investigations have recently been conducted in this region by *Martí et al.* [2009] and the MAGBET project [*Rosell et al.*, 2011], inversion of the PICASSO Phase 1 MT data set focused on the Tajo Basin subsurface. Isotropic 2-D inversion, the common tool in modern MT investigation, was used as the main approach for the data from the MT stations related to Tajo Basin crustal structures, owing to inferred general suitability and validity of the data set with 2-D inversion.

5.1. Start Model

Although 2-D inversions of MT data have been routinely undertaken for over two decades, since *de Groot-Hedlin and Constable* [1990] made the Occam2D code freely available to the academic community in the early 1990s, followed rapidly by Mackie's RLM2DI code (as part of the Geotools package) and *Smith and Booker*'s [1991] RRI, then *Siripunvaraporn and Egbert*'s [2000] REBOCC code, there are still some basic issues associated with their use that requires study. One of these is the starting model used. Commonly, a uniform half space is used, with the notion that such a start model introduces the least bias in the inversion and results in models that are closest, in some sense, to as uniform as possible. An early sensitivity study by *Agarwal et al.* [1993] demonstrated sensitivity to start model and gave some guidelines on start model construction. *Pedersen and Engels* [2005] proposed that initial inversion of the determinants of the MT impedances yields an excellent start model for subsequent 2-D TE and TM mode inversions. However, sensitivity to start model is less appreciated than it should be, but recent studies coming particularly from Chinese scientists [*Bai and Meju*, 2003; *Chen and Wang*, 2006; *Ye et al.*, 2013] are demonstrating this problem. Although not relevant for this paper, such sensitivity to start model is even more acute in 3-D inversion [e.g., *Newman et al.*, 2003], and undertaking multiple inversion runs from different start models is advocated by *Siripunvaraporn* [2012] in his excellent review of 3-D MT inversion. However, ironically, this issue appears at this time to be somewhat better appreciated in 3-D than it is in 2-D.

Thus, rather than starting from a half space, an advanced starting model was used for the inversion for crustal structures, containing layers inferred from seismic studies [e.g., *Banda et al.*, 1981; *ILIHA DSS Group*, 1993; *Julià and Mejía*, 2004; *Dáaz and Gallart*, 2009] and resistivity values derived through averaging of initial inversion results.

5.2. Inversion Steps

Inversion for Tajo Basin crustal structures was carried out using a range of adaptive processes during the inversion. These are all detailed in full in *Schmoldt* [2011], to which the interested reader is referred. Initial inversion steps involved inversion with a range of smoothing parameters (Figure 9), inversion of only TE and of only TM mode data, as well as *sharp boundary* inversion [*WinGLink*, 2005] with predefined changes of electric resistivity along the boundaries of seismically derived layers beneath the Tajo Basin. The subsequent steps that were followed were as follows:

1. During initial inversion steps, four tear zones were applied to maintain separation of the model into upper (0–10 km), intermediate (10–24 km), and lower crust (24–31.5 km) as well as the mantle ($\geq$ 31.5 km) (Note, a tear zone is where changes in conductivity across the boundary do not contribute to the summed roughness measure so can be as discontinuous in conductivity as required to best fit

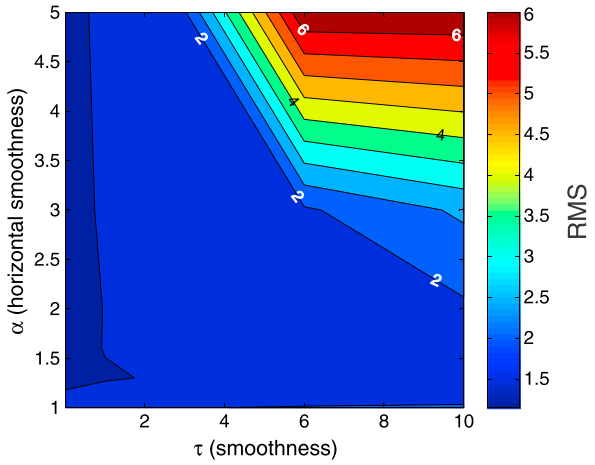

Figure 9. Trade-off between misfit and smoothness of models for the Tajo Basin crustal structures, displayed using an *L* surface plot (a three-dimensional *L* curve equivalent); RMS misfits of the models are indicated by color, with warm colors related to high misfits. Values are obtained through linear interpolation of misfits for 42 inversion models derived with different combinations of the global smoothing parameter (τ) and horizontal smoothing parameter (α).

the data. An example is shown for 1-D in *Jones* [2013] where a tear zone was permitted at the Moho, analogous to what we are doing here);

2. Features were manually removed or their resistivity values were modified in order to test whether they became reestablished in subsequent inversion steps and could therefore be considered data-supported structures;
3. Focused inversions were carried out for specific regions of the subsurface by individually inverting responses from selected stations;
4. Anisotropic 2-D inversions, using the code of *Baba et al.* [2006], were carried out using a range of isotropy parameters (τ_{iso}) in order to test for the existence of possible anisotropic structures.

In the process of determining the final model, multiple models were generated, modified, compared, and subsequently adapted [see *Schmoldt*, 2011]. Presentation of all of these models is too extensive for inclusion in this paper; the major steps in the inversion strategy are listed as points (i) to (iv) above. A more detailed description of the steps and resulting models is given in the PhD thesis of J.-P. Schmoldt [*Schmoldt*, 2011].

For the anisotropic modeling (given the limitation of the code that the axes of anisotropy are required to be parallel and perpendicular to regional strike), even for a relatively low anisotropy regularization constraint ($\tau_{iso} = 10$), anisotropy magnitude in the orthogonal models was overall very low and mostly confined to the surficial conductive layer (cf. Figure 10). These modeling tests demonstrated that the data can be satisfactorily fit to models with an isotropic conductivity in each model cell, and more complicated anisotropic conductivity in some cells does not have to be appealed to. A numerical modeling study we undertook [*Schmoldt and Jones*, 2013] demonstrated the validity of our approach.

5.3. Final Model

The final Tajo Basin crustal model fits the observed MT data very well; the model exhibits an RMS misfit of 1.47 using error floors of 5% for the phases and 10% and 20% for the apparent resistivities of the TM and TE mode data, respectively. A relatively even distribution of the misfit was obtained using focused inversions, which reduced the misfit of respective regions and ensured that the overall model misfit is not controlled by the misfit of a small area within the model (cf. Figure 11). For the final crustal model (Figure 12), all stations

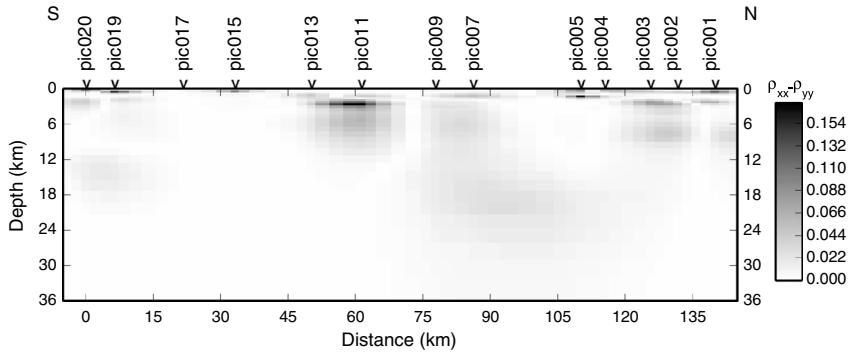

Figure 10. Potential anisotropy of the Tajo Basin crust, modeled using the anisotropic 2-D inversion software `MT2Dinv` [*Baba et al.*, 2006], based on the algorithm by *Rodi and Mackie* [2001] and low isotropic constraints ($\tau_{iso} = 10$).

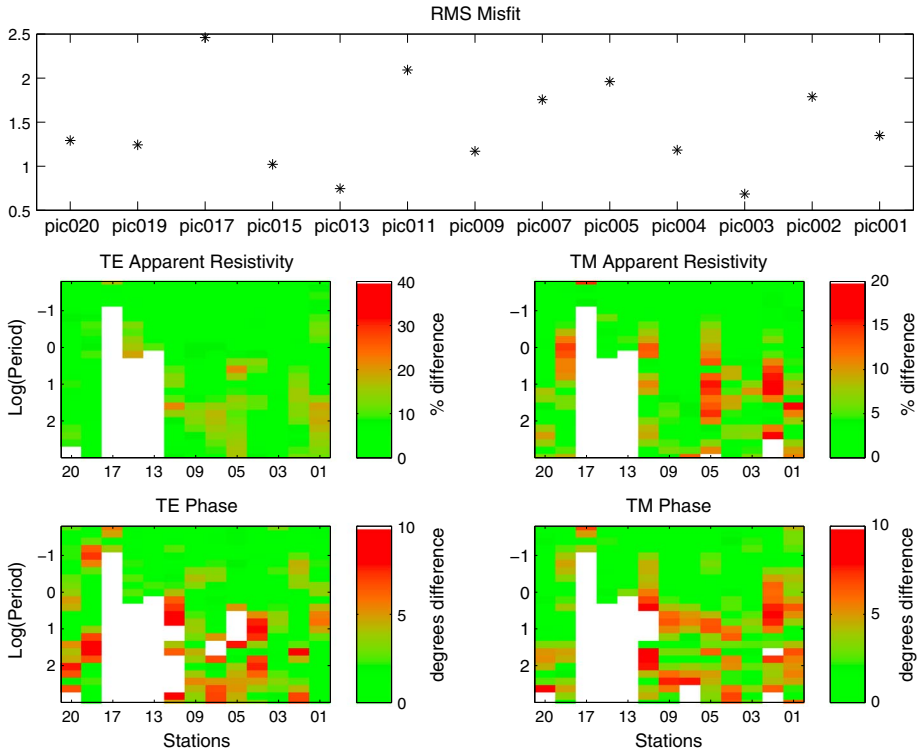

Figure 11. (top) Misfit of the final Tajo Basin crust model, individually broken down into an average for each station, as well as for (middle) apparent resistivity and (bottom) phase of the two modes; due to space restriction, only a selection of station indexes is given at the bottom of apparent resistivity and phase plots. The color scale is set to a range of 2 times the error floor used in the inversion.

exhibit an RMS misfit of 2.5 or less, with a relatively uniform distribution of the misfit for all stations and periods. It should be noted, however, that the response data of stations in close proximity to the DC train line had to be truncated due to high noise levels; thus, structures in this region are less well constrained (indicated by white space in Figure 11).

In order to determine the reliability of resolution of features and regions within the inversion model, sensitivity analysis was carried out following the approach of *Schwalenberg et al.* [2002]. A normalized form of the Jacobian, derived for each cell during inversion, is used to calculate the sensitivity distribution. The resulting sensitivity plot (Figure 13) indicates, first, an overall decrease of sensitivity with depth and, second, a

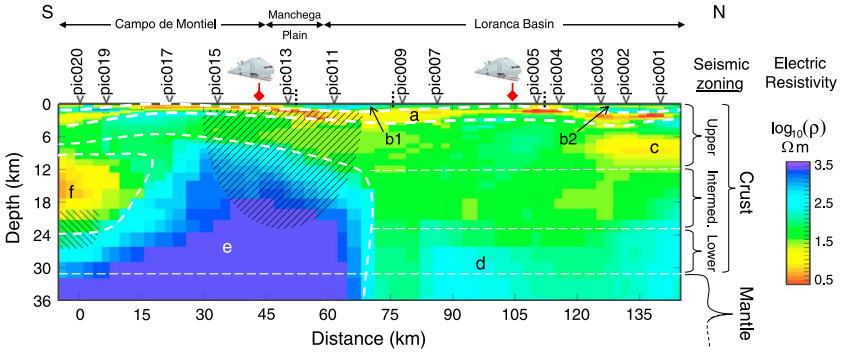

Figure 12. Final model of the electric resistivity distribution at crustal depth beneath the Tajo Basin, derived through inversions of the magnetotelluric PICASSO Phase 1 profile data in the period range 10^{-2}–10^{3} s; see Figure 1 for the profile location. Also shown are the geological regions of the Tajo Basin (based on the USGS EnVision map for Europe, Figure 5), crossover point locations of faults with the PICASSO Phase 1 profile (dotted vertical black lines), different crustal and mantle layers derived by seismic studies in this region (thin white horizontal dashed lines), and regions of low resolution (shaded).

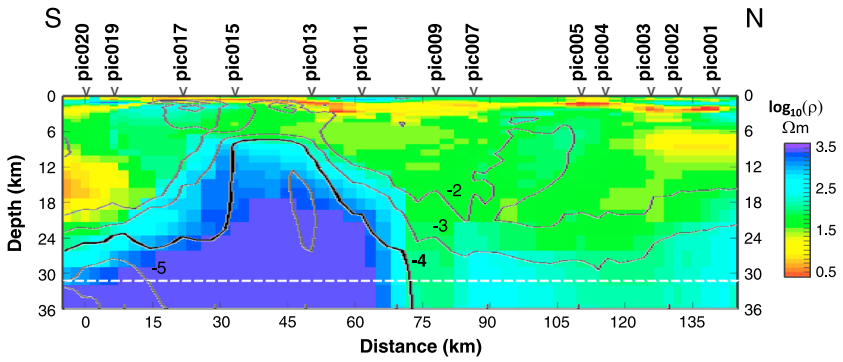

Figure 13. Inversion model of the Tajo Basin crustal structures overlaid by isolines from linear sensitivity analysis following the approach by *Schwalenberg et al.* [2002]; isoline labels are given in terms of logarithmic sensitivity values. For clarity reasons only a selection of isolines is displayed here, of which the thicker isoline (10^{-4}) indicates the threshold value chosen by different authors as the lower limit above which structures of a model are adequately resolved. The dashed white line denotes the crust mantle boundary inferred by seismic studies (see section 2.1 for details).

particularly low sensitivity to the area of the resistor associated with the Iberian Massif (labeled "e" in Figure 12). Whereas the former is due to general attenuation of diffusive EM fields with depth, the latter may be a result of response data truncation for stations in the proximity of the DC train line. However, it is more likely to be due to the inherent problems for induction data in deriving the correct sensitivity to resistive structures using a linearized approach (see below). Lower sensitivity to the region between stations pic005 and pic007 is due to the larger station spacing in the area.

Most structures in the Tajo Basin crust (shallower than 31 km) are above the 10^{-4} sensitivity isoline calculated from the linear sensitivity analysis; a value used by different authors as the threshold above which structures of a model can be assumed to be adequately resolved [e.g., *Schwalenberg et al.*, 2002; *Brasse et al.*, 2002; *Ledo et al.*, 2004]. However, presently, no physical explanation can be found to justify this choice of the limit; therefore, sensitivity results should be considered as a qualitative guide. Furthermore, it was shown by *Ledo et al.* [2004] that linearized sensitivity analysis is less adequate in determining resolution of regions with high resistivity, such as feature "e." The actual resistivity of resistive features usually cannot be determined, but the lower bound can.

In addition to the linearized sensitivity analysis, a number of forward model calculations were performed in which resistivity values of different regions were modified manually in order to examine robustness of the model features in a nonlinear trial-and-error exercise. As a result, values of resistive features in the final model were reduced to the minimum values possible without increasing the RMS misfit of the model.

6. Discussion of Resulting Model

6.1. Near-Surface Conducting Features "a" and "b"

Although the survey was designed for imaging regional structures in the lithospheric mantle down to 100+ km, with, in particular, a site spacing of the order of 20 km generally and 10 km in the region of rapid lateral variation in resistivity, there is nonetheless sensitivity to near-surface features. These near-surface features are identified in the MT data and are well resolved when lying beneath a station, but the geometries of them are relatively poorly resolved between stations, although their exitence is identified. This comes from the inductive response of them when they lie inductively close to a site, but when too far from a site then the response is galvanic only, i.e., due to the charges on the lateral conductivity contrasts.

Close to the surface, down to a depth of around 3 km, a highly conductive structure (labeled "a" in Figure 12) is present throughout the whole length of the Tajo Basin. This surficial conductor is concluded to be caused by either an accumulation of saline fluid in rocks of increased permeability, or by an increase of fluid salinity, or both, at the bottom of the Tertiary and Mesozoic sedimentary layer. Along the profile, the location of this conductor is displaced downward by two somewhat resistive regions labelled "b1" and "b2." The horizontal limits of region "b1," located in the center of the profile (around station pic011), may be related to two faults intersecting the MT profile in the proximity of stations pic009 and pic013 [*de Vicente et al.*, 1996] (indicated by vertical dashed black lines in Figure 12). The northern downward displacement of conductor "a"

(labeled "b2") coincides with the location of a fault between stations pic004 and pic005. However, it is not possible to infer the depth extent of these faults from the MT inversion model. Also, effects caused by the Altomira Range cannot be ruled out as causes for the displacement of conductor "a." Additional information is required to investigate the characteristics of this conductor in more detail.

6.2. Intermediate Crustal Conducting Feature "c"

Besides the two conductors "a" and "c," a relatively homogeneous region of around 100 Ωm is observed in the upper and intermediate crust of the northern region of the profile. The upper crustal conductor "c," situated at the northern end of the MT profile at depths of between 6 km and 12 km, is located in close proximity to the Iberian Range and may potentially represent a related feature at crustal depth. However, mechanisms that can cause such a pronounced anomaly are presently unknown for the Iberian Range region. MT stations at the northern end of the MT profile are located in an area where the Altomira Range and Iberian Range are in close proximity; see Figures 1 and 5 for station locations and local tectonic settings. Accordingly, additional effects owing to the 3-D nature of the respective area might be present. The lateral extent of conductor "c" was investigated in detail using a series of forward models with varying southward extent of the conducting area. The result of the forward modeling analysis yielded a minimum RMS misfit for maximum southward extent of conductor "c" to beneath station pic003, as shown in the model of Figure 12. The base of conductor "c" exhibits some agreement with the base of the seismically defined upper crust, but, due to the low sensitivity of the MT method to regions below a conductor, a correlation between conductor and seismic boundary cannot be conclusively concluded.

6.3. Lower Crustal Resistive Feature "d"

Below anomaly "c," the model exhibits two regions with resistivity values of approximately 100 Ωm and 500 Ωm (i.e., 10^2 and $10^{2.7}$ on the logarithmic scale of Figure 12), of which the bottom region (labeled "d" in Figure 12) may depict the more resistive nature of the Iberian Peninsula lower crust. Structures in the northern region of the MT profile exhibit some agreement with seismically determined vertical changes of velocity.

6.4. Conducting Middle and Lower Crust Beneath the Loranca Basin

The bulk of the crust beneath the Loranca Basin is of the order of some 20–100 Ωm, which is orders of magnitude more conducting than expected for dry, crustal rocks. Indeed, enhanced conductivity in the lower crust is more the norm than the opposite, and there are only a few locations in the world where the rocks are as resistive as expected from laboratory measurements, such as beneath the southern [*Jones and Ferguson*, 2001] and western [*Spratt et al.*, 2009] parts of the Slave Craton of northern Canada, beneath the Rae Craton at the boundary with the Snowbird Tectonic Zone [*Jones et al.*, 2002], also in northern Canada, and beneath the Eastern Indian Craton [*Bhattacharya and Shalivahan*, 2002; *Shalivahan et al.*, 2014], all Archean in age.

As always when we sense a pervasive conductor in the lower crust, we can only be very speculative about its cause as we can never retrieve samples in in situ conditions. Candidates have been proposed by many authors over the last half century to explain the observed enhanced conductivity in the continental lower crust [e.g., *Jones*, 1992; *Brown*, 1994; *Yang*, 2011], and all are contentious and none without objection. The notion of interconnected graphitic thin films [e.g., *Duba and Shankland*, 1982; *Frost et al.*, 1989], a candidate also much promoted for the lithospheric mantle, is discredited by the recent laboratory measurements of *Yoshino and Noritake* [2011]. Aqueous fluids [e.g., *Hyndman and Hyndman*, 1968; *Jones*, 1987; *Hyndman and Shearer*, 1989; *Glover and Vine*, 1994], for a long time the favorite explanation of MT people, does not have broad petrological support [*Yardley and Valley*, 1997], although *Wannamaker* [2000] challenged that view (see response by *Yardley and Valley* [2000]). Aqueous fluids possibly may only be appealed to in active, water-rich environments [e.g., *Li et al.*, 2003], although the two superdeep boreholes, Kontinentales Tiefbohrprogramm (KTB) in Germany [*Emmermann and Lauterjung*, 1997] and Kola Superdeep Borehole in northern Russia [*Kozlovsky*, 1987], both exhibit surprising amounts of free saline fluid at all depths [*Karus et al.*, 1987; *Moller et al.*, 1997]. Partial melts [e.g., *Wannamaker*, 1986; *Partzsch et al.*, 2000a] are an appropriate candidate for the Tibetan crust [e.g., *Li et al.*, 2003; *Gaillard et al.*, 2004] but not for the Iberian lower crust. Sulfides [e.g., *Jones et al.*, 1997] may be a possible candidate, as may graphitized shear zones, a conjecture that we also propose for anomaly "f" (see below). Graphitized shear zones are seen in a number of orogens [e.g., *Korja*, 1993], including in the Variscan orogen in SW Spain [*Pous et al.*, 2004]. Iron oxides, seen in the KTB borehole at some 9 km depth [*Duba et al.*, 1994], may also play a role.

The cause of the enhanced conductivity below the Loranca Basin is open to speculation and could be one or more of the above candidates or could be something else entirely that we have yet to appreciate. We have no constraints we can apply to aid us with any certitude as to why the resistivity of the middle and lower crust below the basin is so low.

6.5. Resistive Crustal Feature "e"

To the south of station pic009, the Tajo Basin crustal model exhibits a massive resistive body (labeled "e" in Figure 12) extending upward to a depth of approximately 10 km below the Manchega Plain and Campo de Montiel region. Unfortunately, resistor "e" is not well constrained in terms of its actual resistivity, as inferred in the linear sensitivity analysis (Figure 13) and by forward modeling examination conducted in the course of the inversion process. As discussed above, the low resolution is due to distortions of the MT responses by DC train line noise in this region requiring truncation of affected stations; the shaded area in Figure 12 indicates the region associated with distortion of the magnetic components, inferred from magnetic transfer function data (Figure 8). In addition, distortion in the electric component may affect longer period responses that are related to deeper structures. Hence, the question arises as to what degree feature "e" originates from the distortion caused by the DC train line or is a real geological feature? The data from sites pic009, pic011, and pic019 are virtually unaffected by DC train noise distortion, and they certainly are sensing a resistive feature at depth. Furthermore, in strong support of a geological feature as the cause of anomaly "e" is the spatial correlation between the vertical resistivity interface (between stations pic009 and pic011) and the lateral change of velocity inferred by seismic tomography data (cf. Figure 14). Feature "e" certainly exists and is resistive, but its detailed geometry and actual resistivity are poorly resolved due to the train noise contamination. It is therefore concluded that resistor "e" relates to the Variscan Iberian Massif basement, whereas the more conductive region to the north represents an area that was probably more affected by Alpine deformation, leading to higher electrical conductivities.

The interface between the two regions of different velocity shown in Figure 2 exhibits a NW-SE orientation, which is in agreement with geoelectric strike direction determined for the Tajo Basin crust. The significant DC train noise contamination on our data from sites at this boundary make its resolution difficult. However, much as for other regions of the world of high resistivity in the crust, the existence of the high-resistivity structures mean that distortions are more severe in the data recorded over them. That the distortions of the data are so strong at these stations is in and of itself prima facie evidence of the existence of the resistive structure; its absence would mean a lesser effect spatially on our data from the distorting noise source.

The modeled downward extent of the resistive region is debatable given the electric noise disturbance from the DC train line. As discussed above, disturbance by this electric noise resulted in complete deletion of long period data from stations pic013 and pic015 and truncation of the responses for stations pic011, pic017, and pic019 at 1500 s. Given that the apparent resistivities for pic011 and pic019 at 1500 is of the order of 200 Ωm in the TE mode and 20 Ωm in the TM mode, penetration below those sites is approximately 200 km in TE and 60 km in TM (Niblett-Bostick depths). Thus, we are somewhat certain of some mantle penetration of the resistive region by one mode (TE), but not of the other mode (TM). Also, geophysical considerations infer lack of existence of a resistive region in the mantle given the seismic low velocity of the mantle in this region derived by *Bijwaard et al.* [1998] and *Amaru* [2007] (Figure 3). A region of increased resistivity and low velocity is counterintuitive, as almost all causes for lowering bulk velocity, like fluids, partial melt, and increased temperature, usually result in a concomitant decrease of electric resistivity. Only very special geological settings may accommodate a low-velocity/high-resistivity region, e.g., the presence of unconnected isolated fluid pockets in a resistive host medium. In a highly porous but impermeable medium, fluid pockets will reduce seismic velocity, which is sensitive to the bulk properties, whereas electric resistivity will remain high owing to the lack of connectivity. As such a geological setting is very uncommon, it is more likely that the resistive body is confined to the crust, and the resistive nature of deeper regions in this model are due to distorted responses by DC train disturbance, off-profile features, or the oblique strike direction of the mantle.

6.6. Conductive Intermediate Crustal Feature "f"

At the southern end of the profile, to the south of station pic017, the model exhibits a region of increased electrical conductivity in the depth range 7–25 km (labeled "f" in Figure 12). Given their similarity in location, anomaly "f" is most likely related to the low-velocity region within the Central Iberian Zone (CIZ) derived in the seismic tomography study by *Villaseñor et al.* [2007] (Figure 2). The seismic anomaly is situated in

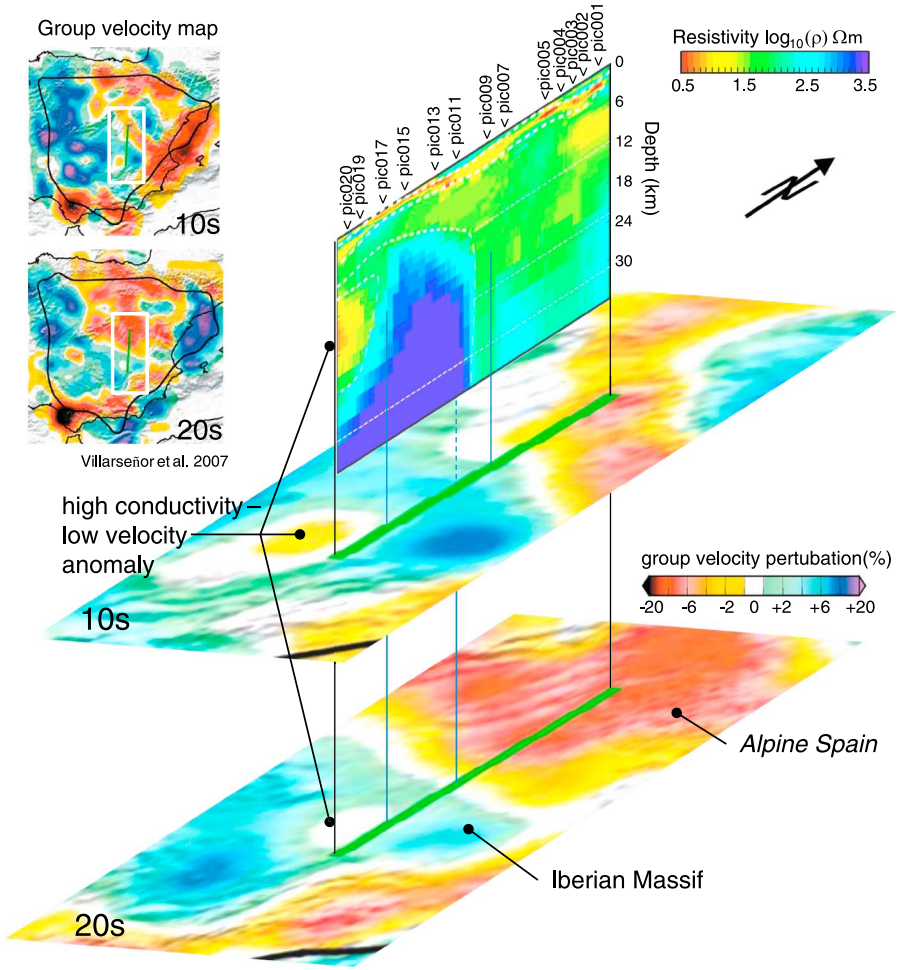

Figure 14. Comparison of the crustal model for the Tajo Basin derived through inversion of the PICASSO Phase 1 MT data and results of the surface wave tomography study by *Villaseñor et al.* [2007]; group velocity maps at 10 s and 20 s are related to structures of the upper 10 km and between 15 and 30 km, respectively. The location of the PICASSO Phase 1 profile is indicated by the thick green line. Correlation between seismic and MT results are observed for the lateral change of resistivity and velocity that are related to the boundary between regions with and without substantial Alpine deformation beneath the Tajo Basin as well as to a high-conductivity/low-velocity anomaly at the southern extent of the profile in the Tajo Basin.

the Campo del Montiel region at the southern edge of the Tajo Basin, with its center located slightly to the west of the MT profile. The assumption that anomaly "f" is due to a geological feature, rather than an end-of-profile inversion artifact, is supported by the response data as well as by the characteristics of the induction vectors (cf. Figure 15). Induction vectors for station pic019 (in Parkinson convention) point directly toward the anomaly, thus indicating current concentration in higher-conductivity bodies in the area. However, induction vectors for stations to the north exhibit a different behavior, pointing in NE (pic017) and NW (pic013 and pic015) directions. Noise from the DC train line, intersecting the MT profile in-between stations pic013 and pic015, distorts magnetic transfer functions of these nearby stations. For station pic017, on the contrary, no straightforward explanation can be proposed for the fact that its induction vectors point away from the low-velocity anomaly. Hence, the existence and location of the conductive feature in the southern Tajo Basin crust is currently based on the MT modeling results.

The seismic anomaly coincident with feature "f" comprises a velocity reduction of up to 4% within the relatively faster region associated with the Iberian Massif. Thus, the anomalous region is inferred to possess high conductivity and low velocity. This rules out most cases of ore bodies as the likely cause of the conductive anomaly, since such features exhibit an increased density that would result in an increase in seismic velocity. The enhanced conductivity of this region is therefore unlikely to originate from interconnected

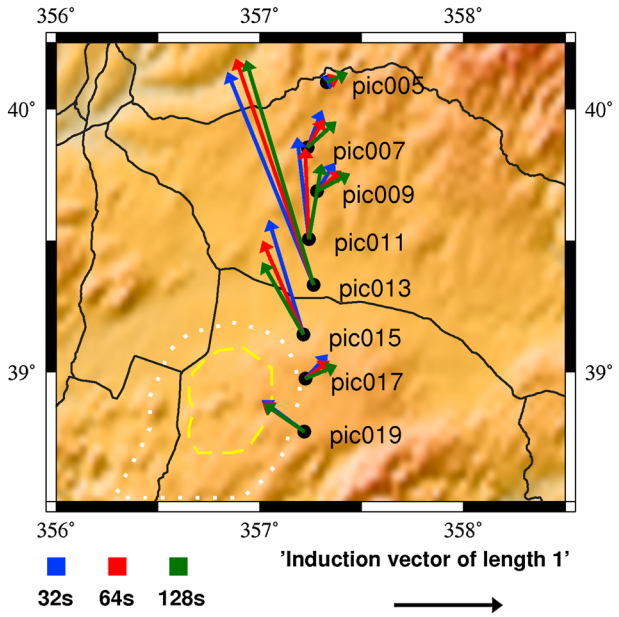

Figure 15. Real induction vectors (Parkinson convention) for periods of 32 s (blue), 64 s (red), and 128 s (green) at PICASSO Phase 1 station in proximity of the high-conductivity-low-velocity anomaly within the Iberian Massif (labeled "f" in Figure 12). The dashed and dotted white and yellow lines indicate the location of the low-velocity anomaly derived by seismic tomography [*Villaseñor et al.*, 2007] (cf. Figure 2). Thin black lines denote the location of DC train lines in the area.

graphite- or sulphide-rich materials in the Variscan igneous and metamorphic CIZ rocks, as inferred by *Pous et al.* [2004] and *Muñoz et al.* [2005] for features in the southwest of the Iberian Peninsula. Potential causes of this anomaly are instead the presence of fluids, partial melting of the middle and lower crust, or remnants of asthenospheric material intruded into the lithosphere, all facilitating low-velocity-high-conductivity characteristics.

A potential source of partial melt in the Tajo Basin crust is remnants of asthenospheric material that were intruded into the lithosphere during volcanic events in Pliocene times. This asthenospheric material hypothesis is supported by the observed volcanism in the Calatrava Volcanic Province (CVP), located to the west of the MT profile and the proposed connection with the trans-Morrocan, western-Mediterranean, European (TMWME) megafault system, located to the east of the profile, forming the source region (cf. Figure 4). *López-Ruiz et al.* [1993] (corroborated by *Cebriá and López-Ruiz* [1995] and *López-Ruiz et al.* [2002]) propose a NW-SE directed connection between the CVP and a section of the TMWME beneath the eastern Betic Mountain Chain, intersecting the MT profile in the area of the Campo de Montiel.

An estimation of the minimum melt fraction required to produce the reduced resistivity of feature "f" can be made using the formulation of *Partzsch et al.* [2000b], who use a modified brick layer model implying a completely interconnected network of fluids that yield results close to the Hashin-Shtrikman upper bound [*Hashin and Shtrikman*, 1962]. For the Tajo Basin subsurface, values of $\sigma_{melt} = 4$ S/m (i.e., $\rho_{melt} = 0.25\,\Omega$m) for the alkaline olivine basalt melt conductivity [*Partzsch et al.*, 2000b, and references therein], and $\sigma_{solid} = 5 \times 10^{-4}$ S/m (i.e., $\rho_{solid} = 2000\,\Omega$m) for the surrounding solid rock (cf. Figure 12) are used. As a result, 1 vol% and 7 vol % are determined as minimum melt fractions for the increased electrical conductivity of feature "f," related to composite conductivity values of 0.04 S/m and 0.2 S/m, i.e., resistivities of ≈25 Ωm and 5 Ωm (cf. Figure 16), respectively.

In the calculation of the required melt fractions discussed above, the host rock matrix is assumed to be dry, and a contribution of water to the composite conductivity is not considered. For inferred P-T conditions of the intermediate crustal Tajo Basin subsurface (≈0.3 GPa and 400°C, [*Tejero and Ruiz*, 2002]) partial melting of dry rocks is implausible [e.g., *Thompson and Connolly*, 1995; *Gaillard*, 2004; *Nover*, 2005; *Yoshino et al.*, 2010]. Surface heat flow expressions corresponding to a significantly increased temperature in the Tajo Basin crust are not observed; surface heat flow values of the Tajo Basin (65–70 mW/m^2) [*Fernandez et al.*, 1998] are equal to or above the global continental average (65 mW/m^2) but lower than surface heat flow of regions with a thin lithosphere (≈80 mW/m^2) [*Pollack et al.*, 1993]. Water would be required to reduce the solidus of local rocks in order to facilitate partial melting. In addition, water increases ion mobility, hence conductivity, of the melt phase [*Gaillard*, 2004] and, in the case of interconnected saline fluids, can further increase conductivity by adding electrolytic conduction effects. Therefore, if water is present in the area of the feature "f," a lower amount of melt is required to produce the electrical conductivity anomaly.

Water in the lower and intermediate Tajo Basin crust could originate from a deeper source region, e.g., from dehydration processes in the slab subducting under the Alboran Domain and the Betic Mountain Chain

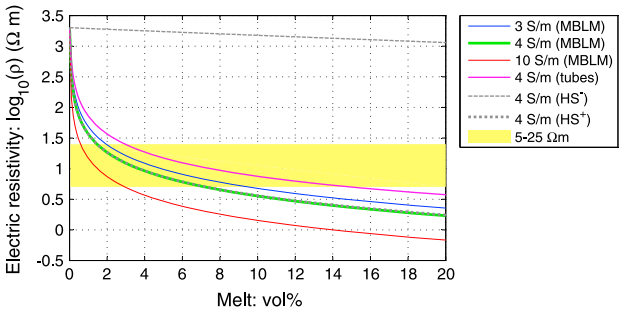

Figure 16. Electric resistivity of a partially molten rock as function of melt fraction; using the modified brick layer model (MBLM) by *Partzsch et al.* [2000b], with melt conductivities of 3 S/m (blue line), 4 S/m (green line), and 10 S/m (red line), the equally spaced conducting (4 S/m) tubes model by *Schmeling* [1986] (purple line), as well as Hashin-Shtrikman extremal bounds [*Hashin and Shtrikman*, 1962] with a conductivity of 4 S/m for the melt phase; the conductivity of the solid phase is set to 5×10^{-1} S/m (2000 Ωm) for all approaches. 4 S/m represents the conductivity of the alkaline olivine basalt [*Partzsch et al.*, 2000b, and references therein] determined as composition for the second volcanic event in the Calatrava Volcanic Province (CVP). The yellow-shaded region indicates the resistivity range for feature "f" in Figure 12.

(Figure 3). Related hydrous phases may have migrated upward into a lithosphere that was weakened by Pliocene indentation events and accumulated at the bottom of an impermeable upper crustal layer. In a similar interpretation, upward migration of fluids originating from dehydration of a subducting slab was reported by *Wannamaker et al.* [2009] as the cause for a lower crustal conductor in Marlborough, New Zealand. Hence, the increased electrical conductivity in the intermediate and lower crust beneath the Campo de Montiel could be due to a combined contribution of water and partial melt.

7. Summary and Conclusions

For the Tajo Basin a sedimentary thickness of approximately 3 km was determined with saline fluid accumulation concluded as source of the electrical conductor at the base of the sedimentary layer. The thickness of the sedimentary layer matches previous seismic results by, among others, *Banda et al.* [1981], *ILIHA DSS Group* [1993], and *Dáaz and Gallart* [2009]. The geoelectric strike direction determined for the Tajo Basin crust, i.e., N40.9°W, is in good agreement with the NNW-SSE direction of the Iberian ranges and faults intersecting the MT profile in this area; vertical extents of the faults, however, could not be determined in this study.

Below the sedimentary layer, a distinct separation within the Variscan basement is evident in terms of electric resistivity. The regions affected by Alpine deformation, situated in the north of the MT profile, exhibit generally a less resistive nature and some indication of layering similar to structures proposed by seismic studies for regions in the proximity to the profile. The interface between the regions with and without substantial Alpine deformation below the profile is located between stations pic009 and pic011 on our profile. Accordingly, this study provides support to the idea of an eastward extension of the Iberian Massif beneath large parts of the southern Tajo Basin, further to the east than what may be inferred from surface geology maps (Figures 1 and 5), confirming results of the surface wave tomography study by *Villaseñor et al.* [2007] (Figure 2).

Within the electrically resistive Iberian Massif, beneath the Campo de Montiel region to the west of the MT profile, a middle to lower crustal conductor was defined that coincides with a low-velocity anomaly imaged by surface wave tomography studies (Figure 14). Based on observed Miocene and Pliocene volcanic events in the Calatrava Volcanic Province (CVP, located to the west of the MT profile) and the proposed source region located to the east of the profile, remnants of asthenospheric partial melt intrusion were identified as the most likely cause of the high-conductivity/low-velocity anomaly. Owing to an insignificant increase of surface heat flow in the region, it is further concluded that conductivity and velocity expressions of the anomaly are increased by a hydrous phase. The hydrous phase may originate from dehydration processes of the subducting slab beneath the Alboran Domain and Betic Mountain Chain.

Acknowledgments
The authors would like to thank the members of the PICASSO Phase 1 fieldwork campaign, namely, Colin Hogg, Clare Horan, Juanjo Ledo, Pierpaolo Moretti, Mark Muller, Gerardo Romano, and Sonja Suckro, for their remarkable support. J.P.S. and A.G.J. would like to acknowledge financial support by the Science Foundation Ireland (Picasso, grant SFI 06/RFP/GEO001 to A.G.J.). The authors further wish to acknowledge the SFI/HEA Irish Centre for High-End Computing (ICHEC) for the provision of computational facilities and support. Reviews of the prior versions of this paper greatly improved it, and we thank all reviewers, one of whom was Gerard Munoz, and the Editor, Onno Oncken.

References

Adetunji, A., I. Ferguson, and A. Jones (2014), Crustal and lithospheric scale structures of the Precambrian Superior-Grenville margin, *Tectonophysics*, *614*, 146–169.

Agarwal, A. K., H. E. Poll, and J. T. Weaver (1993), One-and two-dimensional inversion of magnetotelluric data in continental regions, *Phys. Earth Planet. Inter.*, *81*(1–4), 155–176.

Alonso-Zarza, A., et al. (2002), Tertiary, in *The Geology of Spain*, edited by W. Gibbons and T. Moreno, chap. 13, pp. 293–334, Geol. Soc., London, U. K.

Alvaro, M., R. Capote, and R. Vegas (1979), *Acta Geol. Hispánica*, *14*, 172–177.

Amaru, M. L. (2007), Global travel time tomography with 3-D reference models, PhD thesis, Utrecht Univ., Budapestlaan 4, 3584 CD Utrecht, The Netherlands. [Available at http://igitur-archive.library.uu.nl/dissertations/2007-0202-201924/index.htm, Accessed in 2009.]

Amaru, M. L., W. Spakman, A. Villaseñor, S. Sandoval, and E. Kissling (2008), A new absolute arrival time data set for Europe, *Geophys. J. Int.*, *173*(2), 465–472, doi:10.1111/j.1365-246X.2008.03704.x.

Ancochea, E., and J. Brandle (1982), Alineaciones de volcanes en la región volcánica central Eespañola, *Rev. Geofis.*, *38*, 133–138.

Ancochea, E., A. Giuliani, and I. Villa (1979), Edades radiométricas K-Ar del vulcanismo de la región central Española, *Estudios Geol.*, *35*, 131–135.

Andeweg, B. (2002), Cenozoic tectonic evolution of the Iberian Peninsula: Effects and causes of changing stress fields, PhD thesis, Vrije Univ. Amsterdam, De Boelelaan 1085, 1081 HV Amsterdam, The Netherlands.

Andeweg, B., G. de Vicente, S. A. P. L. Cloetingh, J. Giner, and A. Muñoz-Martín (1999), Local stress fields and intraplate deformation of Iberia: Variations in spatial and temporal interplay of regional stress sources, *Tectonophysics*, *305*(1–3), 153–164, doi:10.1016/S0040-1951(99)00004-9.

Argus, D., and R. Gordon (1991), No-net-rotation model of current plate velocities incorporating plate motion model NUVEL-1, *Geophys. Res. Lett.*, *18*, 2039–2042.

Artemieva, I. M. (2006), Global $1^{\circ} \times 1^{\circ}$ thermal model TC1 for the continental lithosphere: Implications for lithosphere secular evolution, *Tectonophysics*, *416*(1–4), 245–277, doi:10.1016/j.tecto.2005.11.022.

Aurell, M., et al. (2002), Jurassic, in *The Geology of Spain*, edited by W. Gibbons and T. Moreno, chap. 11, pp. 213–253, Geol. Soc., London, U. K.

Bahr, K., and F. Simpson (2002), Electrical anisotropy below slow- and fast-moving plates: Paleoflow in the upper mantle?, *Science*, *295*, 1270–1272.

Baba, K., A. D. Chave, R. L. Evans, G. Hirth, and R. L. Mackie (2006), Mantle dynamics beneath the East Pacific Rise at 17°S: Insights from the mantle electromagnetic and tomography (MELT) experiment, *J. Geophys. Res.*, *111*, B02101, doi:10.1029/2004JB003598.

Bai, D. H., and M. A. Meju (2003), Deep structure of the Longling–Ruili fault undemeath Ruili basin near the Eastern Himalayan syntaxis: Insights from magnetotelluric imaging, *Tectonophysics*, *364*(3–4), 135–146.

Bailey, R. (1970), Inversion of the geomagnetic induction problem, *Proc. R. Soc. A*, *315*(1521), 185–194, doi:10.1098/rspa.1970.0036.

Banda, E., E. Suriñach, A. Aparicio, J. Sierra, and E. Ruiz de la Parte (1981), Crust and upper mantle structure of the central Iberian Meseta (Spain), *Geophys. J. R. Astron. Soc.*, *67*, 779–789.

Banks, C., and J. Warburton (1991), Mid-crustal detachment in the Betic system of Southeast Spain, *Tectonophysics*, *191*(3), 275–289.

Becken, M., O. Ritter, and H. Burkhardt (2008), Mode separation of magnetotelluric responses in three-dimensional environments, *Geophys. J. Int.*, *172*(1), 67–86, doi:10.1111/j.1365-246X.2007.03612.x.

Berdichevsky, M. N. (1999), Marginal notes on magnetotellurics, *Surv. Geophys.*, *20*(3), 341–375.

Berdichevsky, M. N., and V. I. Dmitriev (1976), Distortion of magnetic and electrical fields by near-surface lateral inhomogeneities, *Acta Geod., Geophys. Mon., Hung.*, *11*, 447–483.

Berdichevsky, M. N., V. A. Kuznetsov, and N. A. Palshin (2009), Analysis of magnetovariational response functions, *Izv. Phys. Solid Earth*, *45*(3), 179–198, doi:10.1134/S106935130903001X.

Bhattacharya, B. B., and Shalivahan (2002), The electric moho underneath Eastern Indian craton, *Geophys. Res. Lett.*, *29*(10), 1376, doi:10.1029/2001GL014062.

Bijwaard, H., and W. Spakman (2000), Non-linear global *P*-wave tomography by iterated linearized inversion, *Geophys. J. Int.*, *141*(1), 71–82, doi:10.1046/j.1365-246X.2000.00053.x.

Bijwaard, H., W. Spakman, and R. E. Engdahl (1998), Closing the gap between regional and global travel time tomography, *J. Geophys. Res.*, *103*(B12), 30,055–30,078, doi:10.1029/98JB02467.

Bonadonna, F., and I. Villa (1986), Estudio geochronológico del volcanismo de Las Higueruelas, *Actas Castilla-La Mancha: Espacio y Sociedad*, *3*, 249–253.

Bostick, F. X. (1977), A simple almost exact method of MT analysis, in *Report on Workshop on Electrical Methods in Geothermal Exploration*, edited by S. H. Ward, pp. 174–183, Dept. Geol. Geophys., Univ. of Utah, Salt Lake City.

Brasse, H., P. Lezaeta, V. Rath, K. Schwalenberg, W. Soyer, and V. Haak (2002), The Bolivian Altiplano conductivity anomaly, *J. Geophys. Res.*, *107*(B5), 2096, doi:10.1029/2001JB000391.

Brown, C. (1994), Tectonic interpretation of regional conductivity anomalies, *Surv. Geophys.*, *15*(2), 123–157.

Brum Ferreira, A. (1991), Neotectonics in Northern Portugal: A geomorphical approach, *Z. Geomorphol.*, *82*, 73–85.

Cabral, J. (1989), An example of intraplate neotectonic activity, Vilariç basin, Northeast Portugal, *Tectonics*, *8*(2), 285–303.

Cagniard, L. (1953), Basic theory of the magneto-telluric method of geophysical prospecting, *Geophysics*, *18*, 605–635.

Calvert, A., E. Sandvol, D. Seber, M. Barazangi, S. Roecker, T. Mourabit, F. Vidal, G. Alguacil, and N. Jabour (2000), Geodynamic evolution of the lithosphere and upper mantle beneath the Alboran region of the western Mediterranean: Constraints from travel time tomography, *J. Geophys. Res.*, *105*, 10,871–10,898, doi:10.1029/2000JB900024.

Camfield, P. A., D. I. Gough, and H. Porath (1971), Magnetometer array studies in North-Western United States and South-Western Canada, *Geophys. J. R. Astron. Soc.*, *22*(2), 201–221.

Carbonell, R., V. Sallares, J. Pous, J. J. Dañobeitia, P. Queralt, J. J. Ledo, and G. V. Dueñas (1998), A multidisciplinary geophysical study in the Betic Chain (Southern Iberia Peninsula), *Tectonophysics*, *288*(1–4), 137–152, doi:10.1016/S0040-1951(97)00289-8.

Casas-Sainz, A. M., and G. de Vicente (2009), On the tectonic origin of Iberian topography, *Tectonophysics*, *474*(1–2), 214–235, doi:10.1016/j.tecto.2009.01.030.

Cebriá, J.-M., and J. López-Ruiz (1995), Alkali basalts and leucitites in an extensional intracontinental plate setting: The late Cenozoic Calatrava Volcanic Province (Central Spain), *Lithos*, *35*(1–2), 27–46, doi:10.1016/0024-4937(94)00027-Y.

Cebriá, J.-M., and J. López-Ruiz (1996), A refined method for trace element modelling of nonmodal batch partial melting processes: The Cenozoic continental volcanism of Calatrava, Central Spain, *Geochim. Cosmochim. Acta*, *60*(8), 1355–1366, doi:10.1016/0016-7037(96)00017-8.

Cebriá, J.-M., and M. Wilson (1995), Cenozoic mafic magmatism in Western/Central Europe: A common European asthenospheric reservoir?, *Terra Nova*, *7*, 162.

Chave, A. D., and A. G. Jones (eds.) (2012), *The Magnetotelluric Method: Theory and Practice*, Cambridge Univ. Press, Cambridge, U. K.

Chen, X., and Y. Wang (2006), Constructing reasonable starting model to improve the resolution of MT inversion, *Jianghan Pet. Sci. Technol. (in Chinese)*, *16*(4), 19–22.

Colmenero, J., L. Fernández, C. Moreno, J. Bahamonde, P. Barba, N. Heredia, and F. Gonzáles (2002), Carboniferous, in *The Geology of Spain*, edited by W. Gibbons and T. Moreno, chap. 6, pp. 93–116, The Geol. Soc., London, U. K.

de Groot-Hedlin, C., and S. Constable (1990), Occam's inversion to generate smooth, two-dimensional models from magnetotelluric data, *Geophysics*, *55*(12), 1613–1624.
De Mets, C., R. Gordon, D. Argus, and S. Stein (1994), Effect of recent revision to the geomagnetic reversal time scale on estimate of current plate motion, *Geophys. Res. Lett.*, *21*(20), 2191–2194.
de Vicente, G., and R. Vegas (2009), Large-scale distributed deformation controlled topography along the western Africa-Eurasia limit: Tectonic constrains, *Tectonophysics*, *474*(1–2), 124–143.
de Vicente, G., J. Giner, A. Muñoz-Martín, J. Gonzalez-Casado, and R. Lindo (1996), Determination of present-day stress tensor and neotectonic interval in the Spanish Central System and the Madrid Basin, central Spain, *Tectonophysics*, *266*, 405–424.
de Vicente, G., et al. (2007), Cenozoic thick-skinned and topography evolution of the Spanish Central System, *Global Planet. Change*, *58*(1–4), 335–381.
de Vicente, G., S. Cloetingh, J. V. Wees, and P. Cunha (2011), Tectonic classification of Cenozoic Iberian foreland basins, *Tectonophysics*, *502*(1–2), 38–61, doi:10.1016/j.tecto.2011.02.007.
Dáaz, J., and J. Gallart (2009), Crustal structure beneath the Iberian Peninsula and surrounding waters: A new compilation of deep seismic sounding results, *Phys. Earth Planet. Inter.*, *173*(1–2), 181–190, doi:10.1016/j.pepi.2008.11.008.
Doblas, M., J. López-Ruiz, M. Hoyos, C. Martín, and J. Cebriá (1991), Late Cenozoic indentation/escape tectonics in the eastern Betic Cordilleras and its consequences on the Iberian foreland, *Estudios Geol.*, *47*, 193–205.
Duba, A. G., and T. J. Shankland (1982), Free carbon and electrical conductivity in the Earth's mantle, *Geophys. Res. Lett.*, *9*(11), 1271–1274.
Duba, A. G., S. Heikamp, W. Meurer, G. Nover, and G. Will (1994), Evidence from samples for the role of accessory minerals in lower-crustal conductivity, *Nature*, *367*, 59–61.
Eaton, D. W., A. G. Jones, and I. J. Ferguson (2004), Lithospheric anisotropy structure inferred from collocated teleseismic and magnetotelluric observations: Great Slave Lake shear zone, northern Canada, *Geophys. Res. Lett.*, *31*, L19614, doi:10.1029/2004GL020939.
Egbert, G. (1997), Robust multiple-station magnetotelluric data processing, *Geophys. J. Int.*, *130*, 475–496.
Emmermann, R., and J. Lauterjung (1997), The German continental deep drilling program KTB: Overview and major results, *J. Geophys. Res.*, *102*(B8), 18,179–18,201.
Evans, R. L., M. D. Jegen, X. A. Garcia, T. Matsuno, J. Elsenbeck, and T. W. Worzewski (2010), Magnetotelluric measurements in the Alboran Sea, Abstract C2284 paper presented at AGU Fall Meeting, AGU, San Francisco, Calif., 13-17 Dec.
Fernandez, M., I. Marzan, A. Correia, and E. Ramalho (1998), Heat flow, heat production and lithospheric thermal regime in the Iberian Peninsula, *Tectonophysics*, *291*, 29–53.
Friend, P. F., and C. J. Dabrio (1996), *Tertiary Basins of Spain: The Stratigraphic Record of Crustal Kinematics*, Cambridge Univ. Press, Cambridge, U. K.
Frost, B. R., W. S. Fyfe, K. Tazaki, and T. Chan (1989), Grain-boundary graphite in rocks and implications for high electrical conductivity in the lower crust, *Nature*, *340*(6229), 134–136.
Fullea, J., M. R. Muller, and A. G. Jones (2011), The electrical conductivity of the continental lithospheric mantle: New insights from integrated geophysical and petrological modelling. Application to the Kaapvaal Craton and Rehoboth Terrane, Southern Africa, *J. Geophys. Res.*, *116*, B10202, doi:10.1029/2011JB008544.
Gaillard, F. (2004), Laboratory measurements of electrical conductivity of hydrous and dry silicic melts under pressure, *Earth Planet. Sci. Lett.*, *218*(1–2), 215–228, doi:10.1016/S0012-821X(03)00639-3.
Gaillard, F., B. Scaillet, and M. Pichavant (2004), Evidence for present-day leucogranite pluton growth in Tibet, *Geology*, *32*(9), 801–804.
Gallart, J., G. Fernandez-Viejo, J. Diaz, N. Vidal, and J. Pulgar (1995), Deep structure of the transition between the Cantabrian Mountains and the North Iberian Margin from wide-angle ESCIN data, *Rev. Soc. Geol. España*, *8*(4), 365–382.
Gibbons, W., and T. Moreno (2002a), Introduction and overview, in *The Geology of Spain*, edited by W. Gibbons and T. Moreno, chap. 1, pp. 1–6, Geol. Soc., London, Bath, U. K.
Gibbons, W., and M. T. Moreno (Eds.) (2002b), *The Geology of Spain*, Geol. Soc., London, U. K.
Glover, P. W. J., and F. J. Vine (1994), Electrical conductivity of the continental-crust, *Geophys. Res. Lett.*, *21*(22), 2357–2360.
Goes, S., R. Govers, and P. Vacher (2000), Shallow mantle temperatures under Europe from *P* and *S* wave tomography, *J. Geophys. Res.*, *105*, 11,153–11,169, doi:10.1029/1999JB900300.
Gómez, J., M. Díaz-Molina, and A. Lendínez (1996), Tectono-sedimentary analysis of the Loranca Basin (Upper Oligocene-Miocene, Central Spain): A 'non-sequenced' foreland basin, in *Tertiary basins of Spain: The Stratigraphic Record of Crustal Kinematics*, edited by P. Friend and C. J. Dabrio, chap. 5, pp. 285–294, Cambridge Univ. Press, Cambridge, U. K.
Gómez-Ortiz, D., R. Tejero-López, R. Babín-Vich, and A. Rivas-Ponce (2005), Crustal density structure in the Spanish Central System derived from gravity data analysis (Central Spain), *Tectonophysics*, *403*(1–4), 131–149, doi:10.1016/j.tecto.2005.04.006.
Groom, R. W., and R. C. Bailey (1989), Decomposition of magnetotelluric impedance tensors in the presence of local three-dimensional galvanic distortion, *J. Geophys. Res.*, *94*(B2), 1913–1925.
Gutiérrez-Elorza, M., J. M. García-Ruiz, J. L. Goy, F. J. Gracia, F. Gutiérrez-Santolalla, C. Martí, A. Martín-Serrano, A. Pérez-González, C. Zazo, and E. Aguirre (2002), Quaternary, in *The Geology of Spain*, edited by W. Gibbons and T. Moreno, chap. 14, pp. 335–366, The Geol. Soc., London, U. K.
Gutscher, M.-A., J. Malod, J.-P. Rehault, I. Contrucci, F. Klingelhoefer, L. Mendes-Victor, and W. Spakman (2002), Evidence for active subduction beneath Gibraltar, *Geology*, *30*(12), 1071–1074.
Hamilton, M. P., A. G. Jones, R. L. Evans, S. Evans, C. Fourie, X. Garcia, A. Mountford, and J. E. Spratt (2006), Electrical anisotropy of South African lithosphere compared with seismic anisotropy from shear-wave splitting analyses, *Phys. Earth Planet. Inter.*, *158*(2–4), 226–239, doi:10.1016/j.pepi.2006.03.027.
Hashin, Z., and S. Shtrikman (1962), A variational approach to the theory of the effective magnetic permeability of multiphase materials, *J. Appl. Phys.*, *33*, 3125–3131.
Heise, W., and J. Pous (2001), Effects of anisotropy on the two-dimensional inversion procedure, *Geophys. J. Int.*, *147*(3), 610–621.
Hoernle, K., Y. Zhang, and D. Graham (1995), Seismic and geochemical evidence for large-scale mantle upwelling beneath the Eastern Atlantic and Western and Central Europe, *Nature*, *374*, 34–39.
Hyndman, R. D., and D. W. Hyndman (1968), Water saturation and high electrical conductivity in lower continental crust, *Earth Planet. Sci. Lett.*, *4*(6), 427–432.
Hyndman, R. D., and P. M. Shearer (1989), Water in the lower continental crust—Modeling magnetotelluric and seismic reflection results, *Geophys. J. Int.*, *98*(2), 343–365.
ILIHA DSS Group (1993), A seismic sounding investigation of the lithospheric heterogeneity and anisotropy beneath the Iberian Peninsula, *Tectonophysics*, *221*, 35–51.

Instituto Geográfico Nacional, Seismic Information Service (2010), *Earthquake Catalogue*, Spanish National Geographic Institute, Madrid, Spain. [Available at http://www.ign.es/ign/layoutIn/sismoListadoMapasSismicos.do, Accessed in 2012.]
Jones, A. (1992), Electrical properties of the lower continental crust, in *Continental Lower Crust*, edited by D. Fountain, pp. 81–131, Elsevier, Amsterdam, The Netherlands.
Jones, A., T. Katsube, and P. Schwann (1997), The longest conductivity anomaly in the world explained: Sulphides in fold hinges causing very high electrical anisotropy, *J. Geomagn. Geoelec.*, *49*(12), 1619–1629.
Jones, A. G. (1983a), On the equivalence of the Niblett and Bostick transformations in the magnetotelluric method, *J. Geophys.*, *53*, 72–73.
Jones, A. G. (1983b), The problem of current channelling: A critical review, *Geophys. Surv.*, *6*, 79–122.
Jones, A. G. (1986), Parkinson's pointers' potential perfidy!, *Geophys. J. R. Astron. Soc.*, *87*(3), 1215–1224.
Jones, A. G. (1987), MT and reflection: An essential combination, *Geophys. J. R. Astron. Soc.*, *89*, 7–18.
Jones, A. G. (1988), Static shift of magnetotelluric data and its removal in a sedimentary basin environment, *Geophysics*, *53*(7), 967–978.
Jones, A. G. (2013), Imaging and observing the electrical Moho, *Tectonophysics*, *609*, 423–436.
Jones, A. G., and I. J. Ferguson (2001), The electric Moho, *Nature*, *409*(6818), 331–333.
Jones, A. G., D. Snyder, S. Hanmer, I. Asudeh, D. White, D. Eaton, and G. Clarke (2002), Magnetotelluric and teleseismic study across the Snowbird Tectonic Zone, Canadian Shield: A Neoarchean mantle suture?, *Geophys. Res. Lett.*, *29*(17), 1829, doi:10.1029/2002GL015359.
Jones, A. G., J. Ledo, and I. J. Ferguson (2005), Electromagnetic images of the trans-Hudson orogen: The North American Central Plains anomaly revealed, *Can. J. Earth Sci.*, *42*(4), 457–478.
Jones, A. G., R. L. Evans, and D. W. Eaton (2009), Velocity-conductivity relationships for mantle mineral assemblages in Archean cratonic lithosphere based on a review of laboratory data and Hashin-Shtrikman extremal bounds, *Lithos*, *109*(1–2), 131–143, doi:10.1016/j.lithos.2008.10.014.
Julià, J., and J. Mejía (2004), Thickness and Vp/Vs ratio variation in the Iberian Crust, *Geophys. J. Int.*, *156*(1), 59–72, doi:10.1111/j.1365-246X.2004.02127.x.
Julià, J., J. Vila, and R. Macià (1998), The receiver structure beneath the Ebro Basin, Iberian Peninsula, *Bull. Seismol. Soc. Am.*, *88*(6), 1538–1547.
Karus, E., V. Nartikoyev, O. Bartashevich, G. Gigashvili, S. Ikorsky, M. Pavlova, I. Petersilje, and T. Pisarnitskaya (1987), Gases and organic matter, in *The Superdeep Well of the Kola Peninsula*, edited by Y. Kozlovsky, pp. 243–258, Springer, Berlin, Germany.
Kennett, B. L. N., E. R. Engdahl, and R. Buland (1995), Constraints on seismic velocities in the Earth from travel times, *Geophys. J. Int.*, *122*, 108–125.
Kiyan, D., et al. (2011), Lithospheric-scale geometry of the Atlas Mountains of Morocco revealed by magnetotelluric surveying, in *Geophysical Research Abstracts of the EGU General Assembly*, vol. 13, European Geophysical Union, Vienna, Austria.
Korja, T. (1993), Electrical conductivity distribution of the lithosphere in the central Fennoscandian Shield, *Precambrian Res.*, *64*(1–4), 85–108.
Korja, T. (2007), How is the European lithosphere imaged by magnetotellurics?, *Surv. Geophys.*, *28*, 239–272, doi:10.1007/s10712-007-9024-9.
Koulakov, I., M. K. Kaban, M. Tesauro, and S. Cloetingh (2009), P- and S-velocity anomalies in the upper mantle beneath Europe from tomographic inversion of ISC data, *Geophys. J. Int.*, *179*(1), 345–366, doi:10.1111/j.1365-246X.2009.04279.x.
Kozlovsky, Y. (ed.) (1987), *The Superdeep Well of the Kola Peninsula*, Springer, Berlin, Germany.
Ledo, J., C. Ayala, J. Pous, P. Queralt, A. Marcuello, and J. A. Muñoz (2000), New geophysical constraints on the deep structure of the Pyrenees, *Geophys. Res. Lett.*, *27*(7), 1037–1040, doi:10.1029/1999GL011005.
Ledo, J., A. G. Jones, I. J. Ferguson, and L. Wolynec (2004), Lithospheric structure of the Yukon, northern Canadian Cordillera, obtained from magnetotelluric data, *J. Geophys. Res.*, *109*, B04410, doi:10.1029/2003JB002516.
Ledo, J., A. G. Jones, A. Siniscalchi, J. Campanyà, D. Kiyan, G. Romano, M. Rouai, and TopoMed MT Team (2011), Electrical signature of modern and ancient tectonic processes in the crust of the Atlas mountains of Morocco, *Phys. Earth Planet. Inter.*, *185*, 82–88, doi:10.1016/j.pepi.2011.01.008.
Li, S. H., M. J. Unsworth, J. R. Booker, W. B. Wei, H. D. Tan, and A. G. Jones (2003), Partial melt or aqueous fluid in the mid-crust of Southern Tibet? Constraints from INDEPTH magnetotelluric data, *Geophys. J. Int.*, *153*(2), 289–304.
López-Gómez, J., A. Arche, and A. Pérez-López (2002), Permian and Triassic, in *The Geology of Spain*, edited by W. Gibbons and T. Moreno, chap. 10, pp. 185–212, Geol. Soc. Publ., London, U. K.
López-Ruiz, J., J. M. Cebriá, M. Doblas, R. Oyarzun, M. Hoyos, and C. Martín (1993), Cenozoic intra-plate volcanism related to extensional tectonics at Calatrava, Central Iberia, *J. Geol. Soc.*, *150*(5), 915–922, doi:10.1144/gsjgs.150.5.0915.
López-Ruiz, J., J. M. Cebriá, and M. Doblas (2002), Cenozoic volcanism. I: The Iberian Peninsula, in *The Geology of Spain*, edited by W. Gibbons and T. Moreno, chap. 17, pp. 417–438, Geol. Soc., London, U. K.
Marquis, G., A. G. Jones, and R. D. Hyndman (1995), Coincident conductive and reflective middle and lower crust in Southern British Columbia, *Geophys. J. Int.*, *120*(1), 111–131, doi:10.1111/j.1365-246X.1995.tb05915.x.
Martí, A (2007), A magnetotelluric investigation of geoelectrical dimensionality and study of the central Betic crustal structure, PhD thesis, Univ. of Barcelona, Catalonia, Spain.
Martí, A., P. Queralt, E. Roca, J. Ledo, and J. Galindo-Zaldívar (2009), Geodynamic implications for the formation of the Betic-Rif orogen from magnetotelluric studies, *J. Geophys. Res.*, *114*, B01103, doi:10.1029/2007JB005564.
Martín-Chivelet, J., et al. (2002), Cretaceous, in *Geology of Spain*, edited by W. Gibbons and M. T. Moreno, chap. 12, pp. 255–292, Geol. Soc., London, U. K.
McNeice, G. W., and A. G. Jones (2001), Multisite, multifrequency tensor decomposition of magnetotelluric data, *Geophysics*, *66*(1), 158–173.
Miensopust, M. P., A. G. Jones, M. R. Muller, X. Garcia, and R. L. Evans (2011), Lithospheric structures and Precambrian terrane boundaries in northeastern Botswana revealed through magnetotelluric profiling as part of the Southern African magnetotelluric experiment, *J. Geophys. Res.*, *116*, B02401, doi:10.1029/2010JB007740.
Moller, P., et al. (1997), Paleofluids and recent fluids in the upper continental crust: Results from the German continental deep drilling program (KTB), *J. Geophys. Res.*, *102*(B8), 18,233–18,254.
Moratti, G., and A. Chalouan (eds.) (2006), *Tectonics of the Western Mediterranean and North Africa*, vol. 262, Geological Society Special Publ., London, U. K.
Muñoz, G., W. Heise, A. Paz, E. Almeida, F. Montiero Santos, and J. Pous (2005), New magnetotelluric data through the boundary between the Ossa Morena and CentroIberian Zones, *Geol. Acta*, *3*(3), 215–223.

Muñoz, G., A. Mateus, J. Pous, W. Heise, F. Monteiro Santos, and E. Almeida (2008), Unraveling middle-crust conductive layers in Paleozoic Orogens through 3D modeling of magnetotelluric data: The Ossa-Morena Zone case study (SW Iberian Variscides), *J. Geophys. Res.*, *113*, B06106, doi:10.1029/2007JB004987.

Muñoz-Martín, A., G. de Vicente, and J. M. González-Casado (1994), Análisis tensorial de la deformación superpuesta en el límite oriental de la Cuenca de Madrid, *Cuad. Lab. Xe.*, *19*, 203–214.

Muñoz-Martín, A., S. Cloetingh, G. de Vicente, and B. Andeweg (1998), Finite-element modelling of Tertiary Paleostress fields in the eastern part of the Tajo Basin (central Spain), *Tectonophysics*, *300*, 47–62.

Newman, G. A., S. Recher, B. Tezkan, and F. M. Neubauer (2003), Case history: 3D inversion of a scalar radio magnetotelluric field data set, *Geophysics*, *68*(3), 791–802, doi:10.1190/1.1581032.

Niblett, E. R., and C. Sayn-Wittgenstein (1960), Variation of electrical conductivity with depth by the magneto-telluric method, *Geophysics*, *25*, 998–1008.

Nover, G. (2005), Electrical properties of crustal and mantle rocks: A review of laboratory measurements and their explanation, *Surv. Geophys.*, *26*, 593–651.

Parker, R. L. (1980), The inverse problem of electromagnetic induction: Existence and construction of solutions based on incomplete data, *J. Geophys. Res.*, *85*(B8), 4421–4428, doi:10.1029/JB085iB08p04421.

Parker, R. L. (1982), The existence of a region inaccessible to magnetotelluric sounding, *Geophys. J. R. Astron. Soc.*, *68*, 165–170.

Parker, R. L., and K. A. Whaler (1981), Numerical methods for establishing solutions for the inverse problem of electromagnetic induction, *J. Geophys. Res.*, *86*, 9574–9584.

Parkinson, W. (1959), Direction of rapid geomagnetic variations, *J. R. Astron. Soc.*, *2*, 1–14.

Partzsch, G. M., F. R. Schilling, and J. Arndt (2000a), The influence of partial melting on the electrical behavior of crustal rocks: Laboratory examinations, model calculations and geological interpretations, *Tectonophysics*, *317*(3–4), 189–203.

Partzsch, G. M., F. R. Schilling, and J. Arndt (2000b), The influence of partial melting on the electrical behavior of crustal rocks: Laboratory examinations, model calculations and geological interpretations, *Tectonophysics*, *317*(3–4), 189–203, doi:10.1016/S0040-1951(99)00320-0.

Pedersen, L. B., and M. Engels (2005), Routine 2D inversion of magnetotelluric data using the determinant of the impedance tensor, *Geophysics*, *70*(2), G33–G41.

Pek, J., and F. A. Santos (2006), Magnetotelluric inversion for anisotropic conductivities in layered media, *Phys. Earth Planet. Inter.*, *158*(2–4), 139–158, doi:10.1016/j.pepi.2006.03.023.

Platt, J., and R. Vissers (1989), Extensional collapse of thickened continental lithosphere: A working hypothesis for the Alboran Sea and Gibraltar arc, *Geology*, *17*, 540–543.

Poe, B. T., C. Romano, F. Nestola, and J. R. Smyth (2010), Electrical conductivity anisotropy of dry and hydrous olivine at 8 GPa, *Phys. Earth Planet. Inter.*, *181*(3–4), 103–111.

Pollack, H. N., S. J. Hurter, and J. R. Johnson (1993), Heat flow from the Earth's interior: Analysis of the global data set, *Rev. Geophys.*, *31*(3), 267–280, doi:10.1029/93RG01249.

Pous, J., P. Queralt, J. Ledo, and E. Roca (1999), A high electrical conductive zone at lower crustal depth beneath the Betic Chain (Spain), *Earth Planet. Sci. Lett.*, *167*(1–2), 35–45, doi:10.1016/S0012-821X(99)00011-4.

Pous, J., G. Muñoz, W. Heise, J. C. Melgarejo, and C. Quesada (2004), Electromagnetic imaging of Variscan crustal structures in SW Iberia: The role of interconnected graphite, *Earth Planet. Sci. Lett.*, *217*(3–4), 435–450, doi:10.1016/S0012-821X(03)00612-5.

Pous, J., et al. (2011), On-going magnetotelluric (MT) activities within the Topo-Iberia project, in *Geophysical Research Abstracts*, vol. 13, pp. EGU2011–8811, EGU General Assembly, Copernicus Publications, Germany.

Pulgar, J., G. Gallart, J. Fernandez-Viejo, A. Perez-Estaun, and J. Alvarez-Marron (1996), Seismic image of the Cantabrian Mountains in the western extension of the Pyrenees from integrated ESCIN reflection and refraction data, *Tectonophysics*, *264*, 1–19.

Rebollal, B. M., and A. Pérez-González (2008), Inland aeolian deposits of the Iberian Peninsula: Sand dunes and clay dunes of the Duero Basin and the Manchega Plain. Palaeoclimatic considerations, *Geomorphology*, *102*(2), 207–220, doi:10.1016/j.geomorph.2008.05.009.

Ribeiro, A., M. Kullberg, J. Kullberg, G. Manupella, and S. Phipps (1990), A review of Alpine tectonics in Portugal: Foreland detachment in basement and cover rocks, *Tectonophysics*, *184*, 357–366.

Rikitake, T. (1948), Notes on the electromagnetic induction within the Earth, *Bull. Earthquake Res. Inst. Tokyo*, *24*, 1–9.

Rockwell, T., J. Fonseca, C. Madden, T. Dawson, L. A. Owen, S. Vilanovas, and P. Figueiredo (2009), Palaeoseismology of the Vilariça Segment of the Manteigas-Bragança Fault in northeastern Portugal, in *Palaeoseismology: Historical and Prehistorical Records of Earthquake Ground Effects for Seismic Hazard Assessment*, edited by K. Reicherter, A. M. Michetti, and P. G. Silva, *Geol. Soc. London Spec. Pub.*, 316, 237–258.

Rodi, W., and R. L. Mackie (2001), Nonlinear conjugate gradients algorithm for 2-D magnetotelluric inversion, *Geophysics*, *66*(1), 174–187.

Rosell, O., A. Martí, A. Marcuello, J. Ledo, P. Queralt, E. Roca, and J. Campanyá (2011), Deep electrical resistivity structure of the northern Gibraltar Arc (Western Mediterranean): Evidence of lithospheric slab break-off, *Terra Nova*, *23*(3), 179–186, doi:10.1111/j.1365-3121.2011.00996.x.

Ruiz-Constán, A., J. Galindo-Zaldivar, A. Pedrera, J. A. Arzate, J. Pous, F. Anahnah, W. Heise, F. A. Monteiro Santos, and C. Marín-Lechado (2010), Deep deformation pattern from electrical anisotropy in an arched orogen (Betic Cordillera, western Mediterranean), *Geology*, *38*(8), 731–734, doi:10.1130/G31144.1.

Sato, H., I. Sacks, and T. Murase (1989), The use of laboratory velocity data for estimating temperature and partial melt fraction in the low velocity zone: Comparison with heatflow and electrical conductivity studies, *J. Geophys. Res.*, *94*, 5689–5704.

Schmeling, H. (1986), Numerical models of the influence of partial melt on elastic, anelastic and electric properties of rocks. Part II: Electrical conductivity, *Phys. Earth Planet. Inter.*, *43*, 123–136.

Schmoldt, J.-P. (2011), Multidimensional isotropic and anisotropic investigation of the tajo basin subsurface: A novel anisotropic inversion approach for subsurface cases with oblique geoelectric strike directions, PhD thesis, National University of Ireland, Galway, University Road, Galway, Ireland, in collaboration with the School of Cosmic Physics, Dublin Institute for Advanced Studies, Dublin, Ireland.

Schmoldt, J.-P., and A. G. Jones (2013), A novel anisotropic inversion approach for magnetotelluric data from subsurfaces with orthogonal geoelectric strike directions, *Geophys. J. Int.*, *195*, 1576–1593, doi:10.1093/gji/ggt355.

Schmucker, U. (1973), Regional induction studies: A review of methods and results, *Phys. Earth Planet. Inter.*, *7*(3), 365–378, doi:10.1016/0031-9201(73)90061-7.

Schwalenberg, K., V. Rath, and V. Haak (2002), Sensitivity studies applied to a two-dimensional resistivity model from the Central Andes, *Geophys. J. Int.*, *150*(3), 673–686, doi:10.1046/j.1365-246X.2002.01734.x.

Seber, D., M. Barazangi, A. Ibenbrahim, and A. Demnati (1996), Geophysical evidence for lithospheric delamination beneath the Alboran Sea and Rif-Betic mountains, *Nature*, *379*, 785–790.

Seillé, H., A. Garcia, I. Romero, J. Pous, J. Guimerá, and R. Salas (2012), Crustal structure of the Iberian Chain inferred from magnetotelluric data, in *Geophysical Research Abstracts*, vol. 14, pp. EGU2012–11,992–1, EGU General Assembly, Copernicus Publications, Germany.
Selway, K. (2013), On the causes of electrical conductivity anomalies in tectonically stable lithosphere, *Surv. Geophys.*, *35*, 219–257, doi:10.1007/s10712-013-9235-1.
Serrano, I., J. Morales, D. Zhao, F. Torcal, and F. Vidal (1998), P-wave tomographic images in the central Betics-Alborán Sea (South Spain) using local earthquakes: Contribution for a continental collision, *Geophys. Res. Lett.*, *25*(21), 4031–4034, doi:10.1029/1998GL900021.
Shalivahan, B. B. Bhattacharya, N. V. C. Rao, and V. P. Maurya (2014), Thin lithosphere-asthenosphere boundary beneath Eastern Indian craton, *Tectonophysics*, *612*, 128–133, doi:10.1016/j.tecto.2013.11.036.
Simpson, F. (2001), Resistance to mantle flow inferred from the electromagnetic strike of the Australian upper mantle, *Nature*, *412*, 632–635.
Simpson, F., and K. Bahr (2005), *Practical Magnetotellurics*, Cambridge Univ. Press, Cambridge, U. K.
Siripunvaraporn, W. (2012), Three-dimensional magnetotelluric inversion: An introductory guide for developers and users, *Surv. Geophys.*, *33*(1), 5–27.
Siripunvaraporn, W., and G. Egbert (2000), An efficient data-subspace inversion method for 2-D magnetotelluric data, *Geophysics*, *65*(3), 791–803, doi:10.1190/1.1444778.
Smirnov, M. Y. (2003), Magnetotelluric data processing with a robust statistical procedure having a high breakdown point, *Geophys. J. Int.*, *152*, 1–7, doi:10.1046/j.1365-246X.2003.01733.x.
Smith, J. T., and J. R. Booker (1991), Rapid inversion of two- and three-dimensional magnetotelluric data, *J. Geophys. Res.*, *96*(B3), 3905–3922, doi:10.1029/90JB02416.
Spakman, W., and R. Wortel (2004), A tomographic view on western Mediterranean geodynamics, in *The TRANSMED Atlas—The Mediterranean Region from Crust to Mantle*, edited by W. Canvazza et al., pp. 31–52, Springer, Berlin-Heidelberg.
Spratt, J. E., A. G. Jones, V. A. Jackson, L. Collins, and A. Avdeeva (2009), Lithospheric geometry of the Wopmay orogen from a Slave craton to Bear Province magnetotelluric transect, *J. Geophys. Res.*, *114*, B01101, doi:10.1029/2007JB005326.
Stapel, G. (1999), The nature of isostasy in western Iberia, Vrije Universiteit, Amsterdam, The Netherlands.
Suriñach, E., and R. Vegas (1988), Lateral inhomogeneities of the Hercynian crust in Central Spain, *Phys. Earth Planet. Inter.*, *51*, 226–234.
Tejero, R., and J. Ruiz (2002), Thermal and mechanical structure of the Central Iberian Peninsula lithosphere, *Tectonophysics*, *350*(1), 49–62, doi:10.1016/S0040-1951(02)00082-3.
Tesauro, M., M. K. Kaban, and S. A. P. L. Cloetingh (2009a), How rigid is Europe's lithosphere?, *Geophys. Res. Lett.*, *36*, L16303, doi:10.1029/2009GL039229.
Tesauro, M., M. K. Kaban, and S. A. Cloetingh (2009b), A new thermal and rheological model of the European lithosphere, *Tectonophysics*, *476*(3–4), 478–495, doi:10.1016/j.tecto.2009.07.022.
Thompson, B. A., and J. A. Connolly (1995), Melting of the continental crust: Some thermal and petrological constraints on anatexis in continental collision zones and other tectonic settings, *J. Geophys. Rese.*, *100*(B8), 15,565–15,579, doi:10.1029/95JB00191.
Tikhonov, A. N. (1950), The determination of electrical properties of the deep layers of the Earth's crust, *Doklady Acad. Nauk. SSR*, *73*, 295–297.
Torné, M., M. Fernàndez, M. C. Comas, and J. I. Soto (2000), Lithospheric structure beneath the alboran basin: Results from 3D gravity modeling and tectonic relevance, *J. Geophys. Res.*, *105*(B2), 3209–3228, doi:10.1029/1999JB900281.
Torres, T., P. Garcia Alonso, T. Nestares, and J. Ortiz (1997), Terciario entre la Sierra de Altomira y la Serrania de Cuenca: Aspectos basicos de la paleogeografia cenozoica de la Depresion Intermedia, in *Itinerarios geologicos en el Terciario del centro y este de la Peninsula Iberica*, edited by L. Alcala and A. Alonso-Zarza, pp. 57–70, HC Multimedia, Madrid, Spain.
Torres-Roldan, R., G. Poli, and A. Peccerillo (1986), An early Miocene arc-tholeitic magmatic dike event from the Alboran Sea: Evidence for precollision subduction and back-arc crustal extension in the westernmost Mediterranean, *Geol. Rundsch.*, *75*, 219–234.
Unsworth, M. (2010), Magnetotelluric studies of active continent-continent collisions, *Surv. Geophys.*, *31*, 131–161, doi:10.1007/s10712-009-9086-y.
USGS Energy Resources Program (2010), *Envision, Web Application, v. 1.1.0.*, U.S., Geological Survey, Washington, D. C.
Valladares, M. I., P. Barba, and J. M. Ugidos (2002), Precambrian, in *Geology of Spain*, edited by W. Gibbons and T. Moren, chap. 2, pp. 7–16, Geol. Soc., London, U. K.
Vera, J. A. (ed.) (2004), *Geología de España*, SGE-IGME, Madrid, Spain.
Villaseca, C., H. Downes, C. Pin, and L. Barbero (1999), Nature and composition of the lower continental crust in Central Spain and the granulite-granite linkage: Inferences from granulite xenoliths, *J. Petrol.*, *40*(10), 1463–1496.
Villaseñor, A., Y. Yang, M. H. Ritzwoller, and J. Gallart (2007), Ambient noise surface wave tomography of the Iberian Peninsula: Implications for shallow seismic structure, *Geophysi. Res. Lett.*, *34*, L11304, doi:10.1029/2007GL030164.
Vozoff, K. (1986), *Magnetotelluric Methods*, vol. 5, Society of Exploration Geophysics, Tulsa, Okla.
Vozoff, K. (1987), The magnetotelluric method, in *Electromagnetic Methods in Applied Geophysics—Theory*, vol. 1, pp. 641–712, Soc. Exploration Geophys., Tulsa, Okla.
Wannamaker, P. E. (1986), Electrical conductivity of water-undersaturated crustal melting, *J. Geophys. Res.*, *91*(B6), 6321–6327.
Wannamaker, P. E. (2000), Comment on "The petrologic case for a dry lower crust" by Bruce W. D. Yardley and John W. Valley, *J. Geophys. Res.*, *105*(B3), 6057–6064.
Wannamaker, P. E., G. T. Caldwell, G. R. Jiracek, V. Maris, G. J. Hill, Y. Ogawa, H. M. Bibby, S. L. Bennie, and W. Heise (2009), Fluid and deformation regime of an advancing subduction system at Marlborough, New Zealand, *Nature*, *460*(7256), 733–736, doi:10.1038/nature08204.
Weckmann, U. (2012), Making and breaking of a continent: Following the scent of geodynamic imprints on the African continent using electromagnetics, *Surv. Geophys.*, *33*, 107–134, doi:10.1007/s10712-011-9147-x.
Wiese, H. (1962), Geomagnetische Tiefentellurik. II. Die Streichrichtung der Untergrundstrukturen des elektrischen Widerstandes, erschlossen aus geomagnetischen Variationen (in Germany), *Geofis. Pura Appl.*, *52*, 83–103.
Wilson, M., and H. Downes (1991), Tertiary-quaternary extension-related alkaline magmatism in western and central Europe, *J. Petrol.*, *32*, 811–849.
WinGLink (2005), *WinGLink User'S Guide, 2.07.04 ed.*, Geosystems SRL, 17 Viale Abruzzi, 20131, Milan, Italy. [Available at www.geosystems.net.]
Wu, X., I. J. Ferguson, and A. G. Jones (2005), Geoelectric structure of the Proterozoic Wopmay Orogen and adjacent terranes, Northwest Territories, *Can. J. Earth Sci.*, *981*, 955–981, doi:10.1139/E05-042.
Yang, X. (2011), Origin of high electrical conductivity in the lower continental crust: A review, *Surv. Geophys.*, *32*(6), 875–903.
Yardley, B. W. D., and J. W. Valley (1997), The petrologic case for a dry lower crust, *J. Geophys. Res.*, *102*(B6), 12,173–12,185.

Yardley, B. W. D., and J. W. Valley (2000), Reply [to Comment on 'The petrologic case for a dry lower crust' by Bruce W. D. Yardley and John W. Valley"], *J. Geophys. Res.*, *105*(B3), 6065–6068, doi:10.1029/1999JB900323.

Ye, T., X. B. Chen, and L. J. Yan (2013), Refined techniques for data processing and two-dimensional inversion in magnetotelluric (III): Using the impressing method to construct starting model of 2D magnetotelluric inversion, *Chin. J. Geophys.*, *56*(10), 3596–3606.

Yoshino, T., and F. Noritake (2011), Unstable graphite films on grain boundaries in crustal rocks, *Earth Planet. Sci. Lett.*, *306*(3–4), 186–192.

Yoshino, T., M. Laumonier, E. McIsaac, and T. Katsura (2010), Electrical conductivity of basaltic and carbonatite melt-bearing peridotites at high pressures: Implications for melt distribution and melt fraction in the upper mantle, *Earth Planet. Sci. Lett.*, *295*(3–4), 593–602, doi:10.1016/j.epsl.2010.04.050.